Supplemental materials

RGS2-mediated translational control mediates cancer cell dormancy and tumor relapse

Jaebeom Cho, Hye-Young Min, Ho Jin Lee, Seung Yeob Hyun, Jeong Yeon Sim, Myungkyung Noh, Su Jung Hwang, Shin-Hyung Park, Hye-Jin Boo, Hyo-Jong Lee, Sungyoul Hong, Rang-Woon Park, Young Kee Shin, Mien-Chie Hung, Ho-Young Lee

Supplemental Methods

CFSE dye dilution and PKH26 assays

For CFSE dye dilution assay, parental ACCs (H460 and H1299) and SCCs (H460/PcR, H1299/CsR and H1299/PmR) were labeled with 25 μM CFSE at 37°C for 20 min and then cultured with 1% FBS RPMI 1640 media. The cellular levels of the CSFE fluorescence were monitored by flow cytometry every three days.

PKH26 labeling was performed according to the manufacturer`s instruction (Sigma-Aldrich). H460 cell line or primary lung cancer cells isolated from PDX1 tumors (1-2 x 10^6 cells, each) were labeled with 20 μM PKH26 at room temperature (RT) for 5 min. Stained cells were quenched with serum, seeded in culture plates, and incubated for 7 days. Labeled cells were sorted into $PKH26^{low}$ (lower, ~10%) and $PKH26^{high}$ (upper, ~10%) populations by flow cytometry and used for subsequent experiments.

Cell proliferation assay

Cells (1 x 10^4 cells/well) were seeded in triplicates in 12-well plates and then incubated for 4-5 days. The cells were harvested by trypsinization and counted using a hemocytometer every day.

Mitotic index

CFSE-sorted cells were plated on coverslip and cultured for a day. Attached cells were fixed with 4% paraformaldehyde for 15 min at RT and permeabilized with 0.2% Triton X-100 for 10 min at RT. Immunofluorescence staining to detect the levels of phospho-histone H3 (S10) was performed as described in Methods. To calculate the mitotic index, the number of phospho-Histone H3-positive nuclei were counted and divided by the total number of nuclei, as determined by DAPI-positivity, per image. Five samples were investigated per group, and at least 500 cells were randomly counted per sample in a blinded fashion.

Measurement of energy metabolism

The ECAR and the mitochondrial OCR in cells were measured using an XF Extracellular Flux Analyzer (Seahorse Bioscience, Agilent, Santa Clara, CA, USA) according to the manufacturer's recommended procedure.

Protein synthesis assay

We detected nascent protein synthesis using a Click-iT HPG Alexa Fluor 488 Protein Synthesis Kit (Thermo Fisher Scientific) according to the manufacturer's recommended protocol.

Anchorage-dependent and anchorage-independent colony formation assay

For the anchorage-dependent colony formation assay, cells were seeded onto 12-well plates at a density of 500 cells/well. Cells were then allowed to form colonies or were treated with various concentrations of the test compounds for 10-14 days. The colonies were fixed with 100% methanol, stained with 0.01% crystal violet solution at RT for 1 h, and then washed with deionized water 3-5 times. The colonies were photographed and the number of colonies was counted using ImageJ software (National Institutes of Health, Bethesda, MD, USA) (1).

For the anchorage-independent colony formation assay, 0.5 ml of cell suspension mixed with a sterile 1% agar solution (final concentration of 0.4%) was layered onto a base of 1% solidified agar in 24-well plates (500 cells/well). After adding complete medium with or without test materials to the solidified top agar, the cells were incubated for 2 weeks at 37°C with 5% CO_2. After incubation, the colonies were stained with MTT solution and then photographed, and the number of colonies were counted using ImageJ software.

RT- and real-time PCR

Total RNA was isolated using a phenol-chloroform extraction method, reverse-transcribed, and analyzed by PCR. The primer sequences used for PCR analyses are listed in **Supplemental Table 4**. RT-PCR was performed using 2x MyTaq Red Mix (Bioline, London, UK) and gene-specific primers. The following RT-PCR conditions were applied: an initial denaturation step at 94°C for 5 min; 28-35 cycles of 94°C for 30 sec, 55-60°C for 30 sec, and 72°C for 30 sec; and

a final elongation step at 72°C for 5-7 min. The PCR products were separated by 2% agarose gel electrophoresis and visualized using a Gel Doc EZ System (Bio-Rad Laboratories, Hercules, CA, USA). For real-time PCR analysis, we used a SYBR Green-based qPCR master mix solution (Bioneer, Daejeon, Republic of Korea or Enzynomics, Daejeon, Republic of Korea) and gene-specific primers. All real-time PCR assays were performed on a LightCycler 480 Real-Time PCR System (Roche Applied Sciences, Penzberg, Upper Bavaria, Germany) or an Applied Biosystems 7300 Real-Time PCR System (Thermo Fisher Scientific, Waltham, MA, USA). The following thermocycler conditions for real-time PCR were applied: pre-incubation at 95°C for 15 min; 40-70 cycles of 95°C for 10 sec, 60°C for 15 sec, and 72°C for 30 sec; and a final melt curve analysis to determine reaction specificity. Relative quantification of mRNA expression was performed using the comparative CT (cycle threshold) method as described previously (2).

In silico analysis

We used publicly available datasets deposited in the GEO (National Center for Biotechnology Information): GSE30219 (3) to analyze the associations of RGS2 expression with the histological status and survival of NSCLC patients; GSE8894 (4), GSE41271 (5), GSE42127(6), and GSE63074(7) to analyze the correlation between RGS2 expression and the expression of genes related to cell proliferation and the UPR; and GSE3141 (8), GSE8894, GSE30219, GSE31210 (9), GSE37745 (10), GSE41271, GSE42127, and GSE63074 for GSEA. Raw data comprising gene expression levels and clinical information for each patient sample (such as histology, survival status, and duration of survival) were manually downloaded and analyzed using GraphPad Prism (version 7 and 8, GraphPad Software Inc., San Diego, CA, USA). In the GSE63074 dataset, data categorized as 'Equivalence Study' (n = 172) were used for analysis. Probes used to obtain gene expression values in each dataset were listed in **Supplemental Table 5**. The $RGS2^{high}$ and $RGS2^{low}$ groups were defined based on the median value of the data in each dataset. The association of RGS2 expression with the histological status was analyzed by one-way analysis of variance (ANOVA) followed by

Dunnett's post-hoc test. The normality of the data of each dataset was determined using the D'Agostino-Pearson omnibus test. A Kaplan-Meier survival curve was used to show differences in the survival of NSCLC patients. The log-rank test was used to determine significance.

To determine the correlation coefficient between RGS2 expression and the expression of genes associated with cell proliferation, the Pearson correlation coefficient was calculated for data with a Gaussian distribution, whereas the Spearman correlation coefficient was calculated for data that did not pass the normality test. GSEA was performed using GSEA software (Broad Institute, Massachusetts Institute of Technology, Cambridge, MA, USA) according to the previous reports (11, 12) with GO datasets [obtained from the Molecular Signatures Database (13)] for proliferation and cellular responses to various stimuli, such as oxidative stress and the UPR, as well as datasets for proliferation [Benporath_proliferation (14) and Proliferation signature consisting of 45 common markers of proliferation (15)] and hypoxia activity consisting of 45 HIF target genes (16).

Cell viability assay

Cells (1-2 X 10^3 cells/well in 96-well plates or 2 X 10^4 cells/well in 24-well plates) were incubated for different time intervals or treated with various concentrations of test compounds for 3 days. Cells were harvested and counted using a hemocytometer or further incubated with MTT solution (final 400 μg/ml) for 2-4 h at 37°C. In the MTT assay, formazan products were dissolved in DMSO, and the absorbance was measured at 570 nm. The data are presented as percentages of the control group. The IC_{50} values were calculated using GraphPad Prism (version 7).

Immunoblotting

Cell lysates were obtained using a modified RIPA buffer [50 mM Tris-HCl (pH 7.4), 150 mM NaCl, 1 mM EDTA, 0.25% sodium deoxycholate, 1% Triton X-100] containing various protease and phosphatase inhibitors (100 mM NaF, 5 mM Na_3VO_4, 1 mM PMSF, 1 μg/ml aprotinin, 1 μg/ml leupeptin, and 1 μg/ml pepstatin). Equal amounts (10-30 μg) of cell lysates were

resolved using 8-15% SDS-PAGE and then transferred onto a PVDF membrane. The membranes were blocked with blocking buffer [3% BSA in TBS containing 0.1% Tween-20 (TBST)] for 1 h at RT and then incubated with primary antibodies diluted in blocking buffer (1:1000) overnight at 4°C. The membranes were washed with TBST for 30 min at RT and then incubated with the corresponding secondary antibodies diluted in 3% skim milk in TBST (1:5000-1:10000) for 1-2 h at RT. The membranes were washed several times with TBST for 1 h, and then blots were visualized using an enhanced chemiluminescence (ECL) detection kit (Thermo Fisher Scientific). Densitometric analyses of representative blots were performed using ImageJ software, and the results are included in **Supplemental Figure 19**.

Luciferase reporter assay

Cells were seeded into 24-well plates at a density of 2-2.5 x 10^4 cells/well. Cells were transiently cotransfected with pcDNA3-rLuc-polIRES-fLuc (17) and pCMV-β-gal using JetPRIME transfection reagent (Polyplus-Transfection SA, Illkirch, France). When necessary, cells were further co-transfected with expression vectors or treated with inhibitors. Luciferase assays were performed using Beetle-Juice and Renilla-Juice luciferase assay kits (PJK GmbH, Kleinblittersdorf, Germany). β-Galactosidase activity assays were carried out using β-Gal Juice (PJK GmbH) to normalize for transfection efficiency.

Transfections

To knock down RGS2 expression, cells were transiently transfected with siRNAs targeting RGS2 (5`-GCCCAGAAATGGAGGACATTT-3`) (Shanghai GenePharma, Shanghai, China) using JetPRIME transfection reagent (Polyplus-Transfection SA) according to the manufacturer's instructions. Scrambled siRNAs (5`-TTCTCCGAACGTGTCACGTTT-3`) (Shanghai GenePharma) were used as a negative control. To generate H460 cells stably overexpressing RGS2, cells were transfected with pLX304-RGS2 (purchased from DNASU, Arizona State University, AZ, USA) using Lipofectamine 2000 (Thermo Fisher Scientific), and stably transfected cells were selected with blasticidin. To generate cells transiently

overexpressing RGS2 or ATF4, cells were transfected with either pcDNA3.1-FLAG-RGS2 (subcloned from pLX304-RGS2) or pCGN-mATF4-IRES-GFP (kindly provided by Dr. Sung Hoon Back, University of Ulsan, Ulsan, Republic of Korea) using JetPRIME transfection reagent according to the manufacturer's instructions. To generate cells with stable suppression of RGS2 expression, cells were transduced with lentiviral particles harboring short hairpin RNA (shRNA) clones targeting RGS2 (Sigma-Aldrich) and were then selected with puromycin.

Lentivirus production and transduction

For scrambled (shScr) or RGS2 targeting shRNA (shRGS2) lentivirus production, pCMV-VSV-G and pCMV-dR 8.2 dvpr plasmids were co-transfected to HEK293FT with pLKO.1 Scramble (5`-CCTAAGGTTAAGTCGCCCTCGCTCGAGCGAGGGCGACTTAACCTTAGGTTTTT-3`) or pLKO.1 shRGS2 clones (shRGS2 #1, 5`-CCGGCAGAATATACAAGAAGCTACACTCGAGTGTAGCTTCTTGTATATTCTGTTTTT-3`, shRGS2 #2, 5`-CCGGGAGCCTCATGCTACATGAAATCTCGAGATTTCATGTAGCATGAGGCTCTTTTTG-3`) (Sigma-Aldrich). 12 h after transfection, media were changed to serum-free media. Viral supernatants were collected after 24 and 48 h and filtered through 0.45 μm syringe filter. For lentiviral transduction, cells (1 x 10^5 cells per well in a 6-well plate) were incubated with viral supernatants in the presence of polybrene (8 μg/ml) for 24 h, followed by puromycin selection.

RGS2 knockout using CRISPR/Cas9

Two different guide RNA sequences were selected from CHOPCHOP database (18), and cloned into pCAG-SpCas9-GFP-U6-gRNA vector. H460/PcR cells were plated at a density of 1 x 10^5 cells per well in 6-well plates and transfected with either pCAG-SpCas9-GFP or pCAG-SpCas9-GFP-sgRGS2 clones. Transfection with pCAG-SpCas9-GFP alone served as the negative control. 2 days after transfection, the GFP-positive cells were sorted by flow cytometry to obtain stable RGS2 knockout pools. RGS2 knockout was confirmed by immunoblotting. Sequences of the guide RNA are as follows: sgRGS2 #1: 5`-AGGCAGTGGCCACAAGAGCG-

3`; sgRGS2 #2: 5`-GAAAAGGGTATACAGCTTGA-3`

Cell cycle analysis

Adherent and floating cells were collected and washed with PBS. Cells were fixed with 100% methanol and stained with a 50 μg/ml propidium iodide solution containing 50 μg/ml RNase A for 30 min at RT. Cell cycle analysis was performed by flow cytometry using a FACSCalibur flow cytometer and CellQuest software (BD Biosciences).

SA-β-gal staining

Cells grown on coverslips were fixed with 4% paraformaldehyde. SA-β-gal staining was performed according to the protocol provided by the manufacturer (Cell Signaling Technology).

Sphere formation assay

Cells were seeded in ultra-low attachment 96-well plates (Corning, New York, NY, USA) and cultured in spheroid medium [DMEM-F12 supplemented with 0.4 ml/L B27 supplements (Thermo Fisher Scientific, Waltham, MA, USA), 20 ng/ml EGF, 20 ng/ml bFGF, and 1% antibiotics] at 37°C in 5% CO_2 for 2 weeks. Spheres were photographed using the EVOS FL Cell Imaging System (Thermo Fisher Scientific).

ALDH assay

We performed ALDH assays using an AldeRed ALDH assay kit (Merck Millipore) according to the manufacturer's recommended procedure. Briefly, cells were suspended in AldeRed buffer and stained with AldeRed A588 at 37°C for 40 min. Each group contained a test sample (AldeRed A588 alone) and a control sample [AldeRed A588 plus N,N-diethylaminobenzaldehyde (DEAB)]. The stained cells were analyzed by flow cytometry using a FACSCalibur flow cytometer (BD Biosciences). The sorting gates were established using a negative control sample treated with DEAB. The results were analyzed using FlowJo software (Tree Star, Inc., Ashland, OR, USA, version 10.3).

References

1. Schneider CA, Rasband WS, and Eliceiri KW. NIH Image to ImageJ: 25 years of image analysis. *Nature methods.* 2012;9(7):671-5.

2. Livak KJ, and Schmittgen TD. Analysis of relative gene expression data using real-time quantitative PCR and the 2(T)(-Delta Delta C) method. *Methods.* 2001;25(4):402-8.

3. Rousseaux S, Debernardi A, Jacquiau B, Vitte AL, Vesin A, Nagy-Mignotte H, et al. Ectopic activation of germline and placental genes identifies aggressive metastasis-prone lung cancers. *Sci Transl Med.* 2013;5(186):186ra66.

4. Lee ES, Son DS, Kim SH, Lee J, Jo J, Han J, et al. Prediction of recurrence-free survival in postoperative non-small cell lung cancer patients by using an integrated model of clinical information and gene expression. *Clin Cancer Res.* 2008;14(22):7397-404.

5. Sato M, Larsen JE, Lee W, Sun H, Shames DS, Dalvi MP, et al. Human lung epithelial cells progressed to malignancy through specific oncogenic manipulations. *Mol Cancer Res.* 2013;11(6):638-50.

6. Tang H, Xiao G, Behrens C, Schiller J, Allen J, Chow CW, et al. A 12-gene set predicts survival benefits from adjuvant chemotherapy in non-small cell lung cancer patients. *Clin Cancer Res.* 2013;19(6):1577-86.

7. Huang S, Reitze NJ, Ewing AL, McCreary S, Uihlein AH, Brower SL, et al. Analytical Performance of a 15-Gene Prognostic Assay for Early-Stage Non-Small-Cell Lung Carcinoma Using RNA-Stabilized Tissue. *J Mol Diagn.* 2015;17(4):438-45.

8. Bild AH, Yao G, Chang JT, Wang Q, Potti A, Chasse D, et al. Oncogenic pathway signatures in human cancers as a guide to targeted therapies. *Nature.* 2006;439(7074):353-7.

9. Lietzen N, An LTT, Jaakkola MK, Kallionpaa H, Oikarinen S, Mykkanen J, et al. Enterovirus-associated changes in blood transcriptomic profiles of children with genetic susceptibility to type 1 diabetes. *Diabetologia.* 2018;61(2):381-8.

10. Botling J, Edlund K, Lohr M, Hellwig B, Holmberg L, Lambe M, et al. Biomarker discovery in non-small cell lung cancer: integrating gene expression profiling, meta-analysis, and tissue microarray validation. *Clin Cancer Res.* 2013;19(1):194-204.

11. Subramanian A, Tamayo P, Mootha VK, Mukherjee S, Ebert BL, Gillette MA, et al. Gene set enrichment analysis: a knowledge-based approach for interpreting genome-wide expression profiles. *Proc Natl Acad Sci U S A.* 2005;102(43):15545-50.

12. Mootha VK, Lindgren CM, Eriksson KF, Subramanian A, Sihag S, Lehar J, et al. PGC-1alpha-responsive genes involved in oxidative phosphorylation are coordinately downregulated in human diabetes. *Nat Genet.* 2003;34(3):267-73.

13. Liberzon A, Subramanian A, Pinchback R, Thorvaldsdottir H, Tamayo P, and Mesirov JP.

Molecular signatures database (MSigDB) 3.0. *Bioinformatics.* 2011;27(12):1739-40.

14. Ben-Porath I, Thomson MW, Carey VJ, Ge R, Bell GW, Regev A, et al. An embryonic stem cell-like gene expression signature in poorly differentiated aggressive human tumors. *Nat Genet.* 2008;40(5):499-507.

15. Whitfield ML, George LK, Grant GD, and Perou CM. Common markers of proliferation. *Nat Rev Cancer.* 2006;6(2):99-106.

16. Li B, Qiu B, Lee DS, Walton ZE, Ochocki JD, Mathew LK, et al. Fructose-1,6-bisphosphatase opposes renal carcinoma progression. *Nature.* 2014;513(7517):251-5.

17. Knauf U, Tschopp C, and Gram H. Negative regulation of protein translation by mitogen-activated protein kinase-interacting kinases 1 and 2. *Mol Cell Biol.* 2001;21(16):5500-11.

18. Labun K, Montague TG, Krause M, Torres Cleuren YN, Tjeldnes H, and Valen E. CHOPCHOP v3: expanding the CRISPR web toolbox beyond genome editing. *Nucleic Acids Res.* 2019;47(W1):W171-W4.

Supplemental Table 1. Correlation between 11 commonly upregulated genes of the CSFE^{high} populations and cell proliferation-related genes in GEO datasets.

		CDKN1A		*CDKN1B*		*PCNA*		*MKI67*		*CDK2*	
Dataset		*r*	*P* value	*r*	*P* value	*r*	*P* value	*r*	*P* value	*r*	*P* value
GSE8894	*BCL6*	-0.0071	0.9338	0.02149	0.8024	0.1877	0.0275	0.1956	0.0215	-0.0076	0.9295
	CCPG1	-0.1721	0.0435	0.1227	0.1516	-0.4689	<0.0001	-0.5898	<0.0001	-0.3841	<0.0001
	CLU	-0.1781	0.0366	-0.0652	0.4477	-0.0375	0.6627	0.07929	0.3553	-0.0179	0.8349
	IER5	0.2648	0.0017	0.0179	0.8352	-0.1181	0.1677	-0.1261	0.1405	0.0033	0.9696
	LAMA5	-0.0255	0.767	-0.1575	0.065	0.2226	0.0087	0.2044	0.0162	0.198	0.0199
	MAP3K8	0.1829	0.0318	0.2943	0.0005	-0.0828	0.3341	-0.1234	0.1493	-0.0971	0.2574
	PDCD2L	-0.0366	0.6697	-0.1031	0.2287	0.4351	<0.0001	0.3829	<0.0001	0.3746	<0.0001
	PRDM11	-0.2431	0.0041	-0.0687	0.4237	0.0141	0.8701	0.2069	0.0149	0.02677	0.7553
	RGS2	0.1879	0.0274	0.2560	0.0024	-0.3413	<0.0001	-0.3199	0.0001	-0.2477	0.0034
	SIX3	-0.1493	0.0805	-0.1478	0.0836	0.0849	0.3219	0.2227	0.0087	0.1778	0.1687
	ZNF703	0.0549	0.5228	-0.1916	0.0244	0.3478	<0.0001	0.3642	<0.0001	0.1653	0.0526
GSE41271	*BCL6*	0.0013	0.9834	-0.0547	0.3665	0.0887	0.1424	-0.0879	0.1462	-0.0418	0.4905
	CCPG1	-0.0009	0.9887	0.2575	<0.0001	-0.1164	0.0538	-0.4863	<0.0001	-0.4102	<0.0001
	CLU	-0.0339	0.5757	-0.1128	0.0617	-0.0409	0.499	0.0106	0.8608	-0.0233	0.7005
	IER5	0.2766	<0.0001	-0.0107	0.8594	0.0342	0.5725	0.0941	0.1196	0.044	0.4674
	LAMA5	-0.3762	<0.0001	-0.1992	0.0009	0.1039	0.0854	0.1566	0.0093	0.007	0.9081
	MAP3K8	0.2227	0.0002	0.1517	0.0118	0.0158	0.7937	-0.3003	<0.0001	-0.1719	0.0042
	PRDM11	0.0164	0.7868	-0.0458	0.4491	-0.1853	0.002	0.0009	0.9882	-0.0534	0.3774
	RGS2	0.2681	<0.0001	0.2761	<0.0001	-0.3065	<0.0001	-0.3307	<0.0001	-0.3230	<0.0001
	SIX3	-0.0064	0.9162	-0.0244	0.6868	-0.0658	0.2766	0.1364	0.0237	0.0081	0.894
	ZNF703	0.0278	0.6458	0.0876	0.1473	0.0525	0.3863	0.0269	0.6569	0.0515	0.3953
GSE42127	*BCL6*	0.0098	0.8975	-0.1071	0.1571	-0.001	0.9895	-0.0848	0.2633	-0.0848	0.2634
	CCPG1	0.0126	0.8679	0.281	0.0002	-0.037	0.626	-0.4759	<0.0001	-0.3962	<0.0001
	CLU	-0.0481	0.526	0.0283	0.7089	-0.0603	0.4268	0.0181	0.8111	-0.1062	0.1608
	IER5	0.3079	<0.0001	0.0187	0.8055	0.0139	0.8549	0.0113	0.8818	-0.0156	0.8374
	LAMA5	0.0752	0.3213	-0.4143	<0.0001	-0.2602	0.0005	0.1197	0.1135	0.0009	0.9907
	MAP3K8	0.1505	0.0462	0.2035	0.0067	0.031	0.6828	-0.2605	0.0005	-0.1294	0.0871
	PRDM11	0.0419	0.5812	-0.0124	0.8707	-0.1768	0.0189	-0.0215	0.7772	-0.0279	0.7132
	RGS2	0.2182	0.0036	0.2579	0.0006	-0.3349	<0.0001	-0.2532	0.0007	-0.2292	0.0022
	SIX3	0.0035	0.9636	-0.0465	0.5399	-0.1388	0.0662	-0.0148	0.8452	-0.085	0.2617
	ZNF703	0.1135	0.1337	0.0504	0.5066	0.0365	0.631	-0.0563	0.4579	-0.0354	0.6405
GSE63074	*BCL6*	0.0621	0.4182	0.0603	0.4320	-0.2121	0.0052	-0.1208	0.1145	-0.0610	0.4265
	CCPG1	0.3107	<0.0001	0.2694	0.0004	-0.3388	<0.0001	-0.4182	<0.0001	-0.2409	0.0015
	CLU	0.2530	0.0008	0.0290	0.7060	0.0065	0.9326	0.0410	0.5933	0.1174	0.1251
	IER5	0.3866	<0.0001	0.0024	0.9755	0.1614	0.0344	0.1129	0.1402	0.1613	0.0345
	LAMA5	-0.0872	0.2554	-0.2850	0.0002	0.0982	0.2000	0.0613	0.4241	-0.0056	0.9418
	MAP3K8	0.4122	<0.0001	0.3445	<0.0001	-0.3377	<0.0001	-0.3782	<0.0001	-0.2521	0.0008
	PDCD2L	-0.3747	<0.0001	-0.2740	0.0003	0.6444	<0.0001	0.5897	<0.0001	0.5571	<0.0001
	PRDM11	-0.0326	0.6717	-0.2918	0.0001	-0.0384	0.6168	0.0355	0.6439	0.0132	0.8635
	RGS2	0.4255	<0.0001	0.3695	<0.0001	-0.4062	<0.0001	-0.4083	<0.0001	-0.2834	<0.0001
	SIX3	-0.1677	0.0279	-0.1900	0.0126	-0.0157	0.8378	0.2852	0.0001	0.1274	0.0958
	ZNF703	0.0680	0.3753	-0.1067	0.1636	0.0157	0.8379	0.1154	0.1316	-0.0435	0.5706

Supplemental Table 2. Clinicopathological features of tissue microarray (TMA) specimens.

No.	Age	Sex	Pathology diagnosis	TNM	Grade
1	58	F	Adenocarcinoma	T2bN0M0	G3
2	63	F	Adenocarcinoma	T2aNxM0	G2-G3
3	67	M	Adenocarcinoma	T2aN2M0	G2
4	59	F	Adenocarcinoma, partly bronchiolo-alveolar carcinoma	T1bNxM0	G2
5	60	F	Adenocarcinoma	T1bNxM0	G2
6	42	F	Bronchiolo-alveolar carcinoma	T2aNxM0	G2
7	61	M	Adenocarcinoma	T2bN3M0	G3
8	58	F	Adenocarcinoma	T3N0M0	G1-G2
9	62	F	Bronchiolo-alveolar carcinoma	T1aNxM0	G1
10	60	M	Adenocarcinoma	T3N1M0	G2
11	61	M	Adenocarcinoma	T2aN0M0	G2-G3
12	81	F	Adenocarcinoma	T2aN1M0	G2
13	84	M	Adenocarcinoma, partly bronchiolo-alveolar carcinoma	T2bN0M0	G1-G2
14	60	F	Adenocarcinoma	T1aNxM0	G2
15	65	M	Adenocarcinoma	T2aN2M0	G2
16	50	F	Adenocarcinoma	T1bNxM0	G2
17	64	M	Adenocarcinoma	T1bN0M0	G2
18	74	M	Mucinous adenocarcinoma	T1aM0	G3
19	64	M	Adenocarcinoma	T2aN1M0	G2
20	25	F	Mucoepidermoid carcinoma	T3N0M0	G3
21	53	F	Adenocarcinoma, partly bronchiolo-alveolar carcinoma	T1bN0M0	G1
22	52	M	Adenocarcinoma	T2aN2M0	G2
23	37	M	Adenocarcinoma	T2aN0M0	G2
24	73	F	Adenocarcinoma, partly bronchiolo-alveolar carcinoma	T2bNxM0	G2
25	55	M	Adenocarcinoma	T2bN2M0	G2
26	50	F	Adenocarcinoma	T1aN0M0	G2
27	40	M	Adenocarcinoma	T1bNxM0	G2
28	58	M	Adenocarcinoma	T2aN0M0	G3
29	56	F	Adenocarcinoma	T4N2M0	G2
30	62	F	Adenocarcinoma	T1bNxM0	G2
31	57	M	Adenocarcinoma	T2aNxM0	G2
32	80	F	Bronchiolo-alveolar carcinoma	T2aM0	G1
33	61	M	Adenocarcinoma, partly bronchiolo-alveolar carcinoma	T2bN0M0	G1-G2
34	56	F	Adenocarcinoma, partly bronchiolo-alveolar carcinoma	T2aN0M0	G2
35	65	M	Adenocarcinoma	T3N2M0	G3
36	67	F	Adenocarcinoma	T1aN0M0	G2
37	50	M	Adenocarcinoma, partly bronchiolo-alveolar carcinoma	T2aN0M0	G3
38	50	M	Adenocarcinoma	T2N0M0	G2
39	66	F	Adenocarcinoma	T2aN0M0	G1
40	68	F	Adenocarcinoma	T2aN0M0	G1

Supplemental Table 3. Antibodies used in this study.

Target	Vendor	Catalog No.	Clone	Application
4E-BP-1	Cell Signaling Technology	9452		Immunoblotting
Actin	Santa Cruz Technology	sc-1615	C-11	Immunoblotting
β-Actin	Santa Cruz Technology	sc-47778	C4	Immunoblotting
Akt	Cell Signaling Technology	9272		Immunoblotting
ATF4	Cell Signaling Technology	11815	D4B8	Immunoblotting
ATF4	Proteintech	10835-1-AP		Immunoblotting Immunoprecipitation Immunohistochemistry
CDK4	Santa Cruz Biotechnology	sc-260	C-22	Immunoblotting
Cleaved caspase-3	Cell Signaling Technology	9661		Immunoblotting Immunohistochemistry
Cleaved PARP	BD Biosciences	552596		Immunoblotting
Cyclin D1	Santa Cruz Biotechnology	sc-753	H-295	Immunoblotting
eIF2α	Santa Cruz Biotechnology	sc-11386	FL-315	Immunoblotting
ERK	Cell Signaling Technology	9102		Immunoblotting
GADD153/ CHOP	Santa Cruz Biotechnology	sc-7351	B-3	Immunoblotting
GADD34	Santa Cruz Biotechnology	sc-824	S-20	Immunoblotting
His-Tag	Santa Cruz Biotechnology	sc-8036	H-3	Immunoblotting
Ki67	Abcam	ab15580		Immunofluorescence
LC3B	Cell Signaling Technology	2775		Immunoblotting
mTOR	Cell Signaling Technology	2983	7C10	Immunoblotting
OctA-probe	Santa Cruz Biotechnology	sc-166355	H-5	Immunoprecipitation Immunoblotting
p21	Cell Signaling Technology	2947	12D1	Immunoblotting
p27	Santa Cruz Biotechnology	sc-528	C-19	Immunoblotting

p38	Santa Cruz Biotechnology	sc-535	C-20	Immunoblotting
PCNA	Abcam	ab29	PC10	Immunoblotting
PERK	Cell Signaling Technology	3192	C33E10	Immunoblotting
phospho-4E-BP-1 (S65)	Cell Signaling Technology	9455		Immunoblotting
phospho-Akt (S473)	Cell Signaling Technology	4060	D9E	Immunoblotting
phospho-ERK (T202/Y204)	Cell Signaling Technology	9106	E10	Immunoblotting
phospho-eIF2α (S51))	Cell Signaling Technology	9721		Immunoblotting
phospho-Histone H3 (S10)	Cell Signaling Technology	53348	D7N8E	Immunofluorescence
phospho-mTOR (S2448)	Cell Signaling Technology	2971		Immunoblotting
phospho-p38 (Y182)	Santa Cruz Biotechnology	sc-7973	D-8	Immunoblotting
phospho-p70S6K (T389)	Cell Signaling Technology	9205		Immunoblotting
phospho-PERK (S713)	BioLegend	649401		Immunoblotting
RGS2	Santa Cruz Biotechnology	sc-100761	BC-43	Immunoblotting Immunoprecipitation Immunofluorescence
RGS2	Proteintech	10678-1-AP		Immunoblotting Immunohistochemistry
Ubiquitin	Santa Cruz Biotechnology	sc-8017	P4D1	Immunoblotting
HRP-conjugated anti-mouse IgG	GeneTex	GTX213111-01		Immunoblotting
HRP-conjugated anti-rabbit IgG	GeneTex	GTX213110-01		Immunoblotting
HRP-conjugated anti-goat IgG	GeneTex	GTX232040-01		Immunoblotting
Alexa Fluor 488-conjugated anti-rabbit IgG	Thermo Fisher Scientific	A21206		Immunofluorescence
Alexa Fluor 594-conjugated anti-mouse IgG	Thermo Fisher Scientific	A21203		Immunofluorescence
Biotinylated anti-rabbit IgG	Vector Laboratories	BA-1000		Immunohistochemistry

Supplemental Table 4. Primer sequences used in this study.

Gene	Forward sequence (5´-3´)	Reverse sequence (5´-3´)	Application
RGS2	GAAGCGAGAAAAGATGAAACGG	GAGGACAGCTTTTGGGGTG	RT-PCR
ACTB	ACTACCTCATGAAGATC	GATCCACATCTGCTGGAA	RT-PCR
RGS2	ATGAAGCCTTCTCCTGAGGAA	GGGTAGCAGCTCGTCAAATGC	Real-time PCR
EIF2AK3	AATGCCTGGGACGTGGTGGC	TGGTGGTGCTTCGAGCCAGG	Real-time PCR
DDIT3	GGAGCATCAGTCCCCCACTT	TGTGGGATTGAGGGTCACATC	Real-time PCR
PPP1R15A	CCCAGAAACCCCTACTCATGATC	GCCCAGACAGCCAGGAAAT	Real-time PCR
ATF6	ATGAAGTTGTGTCAGAGAACC	CTCTTTAGCAGAAAATCCTAG	Real-time PCR
HSPA5	CATGGTTCTCACTAAAATGAAAGA	GCTGGTACAGTAACAACTG	Real-time PCR
ERO1B	TTCTGGATGATTGCTTGTGTGAT	GGTCGCTTCAGATTAACCTTGT	Real-time PCR
HSP90B1	TACCCACATCTGCTCCACGTG	ACCAAGCTTGATGTTGGTAC	Real-time PCR
DNAJB11	CCTCGTCAGCAAGACAGAAAT	ATTAGGGCATTCGTCGCAGAC	Real-time PCR
XBP1	CCTGGTTGCTGAAGAGGAGG	CCATGGGGAGATGTTCTGGAG	Real-time PCR
XBP1(spliced)	CGCTTGGGGATGGATGCCCTG	CCTGCACCTGCTGCGGACT	Real-time PCR
SEL1L	CTCGCTAACAGGAGGCTCAGTA	CATGGCATGTGAATTGCCAG	Real-time PCR
CANX	AAGCCAAGAAAGACGATACCGA	GCCCGAGACATCAACACAAGT	Real-time PCR
ERN1	TGCTTAAGGACATGGCTACCATCA	CTGGAACTGCTGGTGCTGGA	Real-time PCR
EDEM1	TGCAATGAAGGAGAAGGAGA	TCCTATCAGCACCTGCAGTC	Real-time PCR
P4HB	ACGCCACGGAGGAGTCTG	TCTTCAGCCAGTTCACGATGTC	Real-time PCR
SYVN1	CTGGGCATCCTGGACTTCCTC	GAGCACCATCGTCATCAGGA	Real-time PCR
AMFR	TTCCACAACTCCTGTCTTCG	CTGCTGCTACAGGAACCAAA	Real-time PCR
KDELR3	TCCGCCTGGAGTTTCTTCTG	AAGAGCTGGGGCAGGATAGC	Real-time PCR
SNAI1	ACCACTATGCCGCGCTCTT	GGTCGTAGGGCTGCTGGAA	Real-time PCR
SNAI2	AACAGAGCATTTGCAGACAGGTC	GCTACACAGCAGCCAGATTCC	Real-time PCR
TWIST1	TGTCCGCGTCCCACTAGC	TGTCCATTTTCTCCTTCTCTGGA	Real-time PCR
CDH1	GAACAGCACGTACACAGCCCT	GCAGAAGTGTCCCTGTTCCAG	Real-time PCR
POUSF1	TGCAGCAGATCAGCCACATC	CTCGGACCACATCCTTCTCG	Real-time PCR
NANOG	CCTCCTCCATGGATCTGCTTATTCA	CAGGTCTTCACCTGTTTGTAG	Real-time PCR
SOX2	AACCAGCGCATGGACAGTTA	ATCATGCTGTAGCTGCCGTT	Real-time PCR
HMBS	CATGTCTGGTAACGGCAATG	GTACGAGGCTTTCAATGTTG	Real-time PCR
ACTB	TCATTCCAAATATGAGATGCGTTG	TAGAGAGAAGTGGGGTGGCT	Real-time PCR

Supplemental Table 5. List of probes used to obtain gene expression values in GEO datasets.

Dataset	Gene	Probe
GSE3141, GSE30219	RGS2	202388_at
GSE8894, GSE63074	BCL6	203140_at
	CCPG1	221156_x_at
	CLU	1559228_at
	IER5	218611_at
	LAMA5	210150_s_at
	MAP3K8	205027_s_at
	PDCD2L	224467_s_at
	PRDM11	220571_at
	RGS2	202388_at
	SIX3	206634_at
	ZNF703	222760_at
	CDKN1A	202284_s_at
	CDKN1B	209112_at
	CDK2	204252_at
	MKI67	212023_s_at
	PCNA	201202_at
GSE41271, GSE42127	BCL6	ILMN_1746053
	CCPG1	ILMN_1746053
	CLU	ILMN_1667058
	IER5	ILMN_1721833
	LAMA5	ILMN_1773567
	MAP3K8	ILMN_1741159
	PRDM11	ILMN_1765218
	RGS2	ILMN_2197365
	SIX3	ILMN_1799076
	ZNF703	ILMN_2415128
	CDKN1A	ILMN_1784602
	CDKN1B	ILMN_2196347
	CDK2	ILMN_1665559
	CCNE1	ILMN_1795852
	MKI67	ILMN_1734827
	PCNA	ILMN_1706958

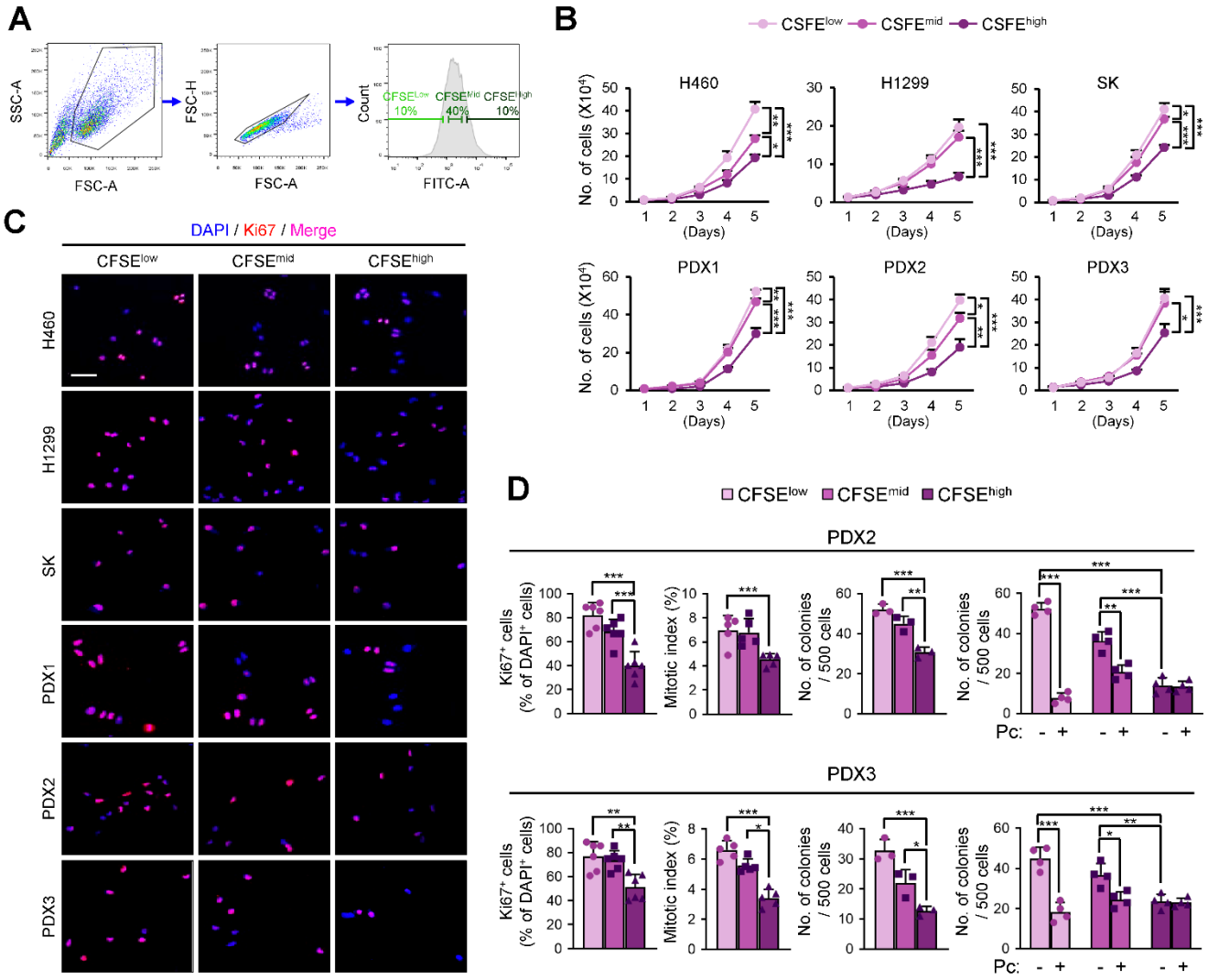

Supplemental Figure 1. Cellular properties of CFSE^{high} slow-cycling cell population. (**A**) Gating strategy to isolate CFSE^{low} (~10%), CFSE^{mid} (~35-40%) and CFSE^{high} (~10%) populations. (**B** and **C**) Changes in cell proliferation (**B**) and Ki67 positivity (**C**) of the CFSE^{low}, CFSE^{mid}, and CFSE^{high} populations isolated from NSCLC cell lines or PDX-derived primary tumor cells. (**C**) Representative immunofluorescence images are shown. Scale bar, 50 μm. (**D**) Basal level of Ki67 positivity, mitotic index, anchorage-dependent colony formation, and resistance to chemotherapy in the anchorage-independent colony formation assay in the CFSE^{low}, CFSE^{mid}, and CFSE^{high} populations isolated from additional two different PDX tumors (PDX2, PDX3). The data are presented as the means ± SDs. n = 3 for **B**; n = 3-6 for **D**. *P < 0.05 and ***P < 0.001, as determined by one-way ANOVA with Dunnett's post-hoc test (**B** and **D**).

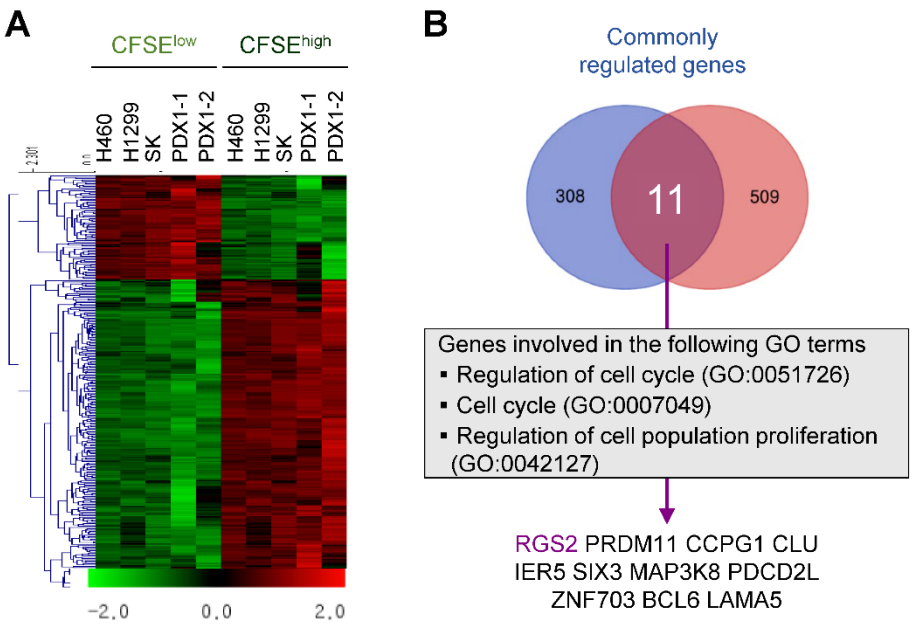

Supplemental Figure 2. Identification of the significantly enriched transcriptomes in SCCs of NSCLC cell lines or NSCLC patient-derived tumors compared to the corresponding ACCs. (**A**) Heatmap showing hierarchical clustering of gene expression profiles in CFSE^{high} cells compared with CFSE^{low} cells. (**B**) Venn diagram showing overlapped genes between 319 significantly changed genes in all CFSE^{high} populations and genes associated with one of the following GO terms: cell cycle (GO: 0007049), regulation of cell population proliferation (GO: 0042127), and regulation of cell cycle (GO: 0051726).

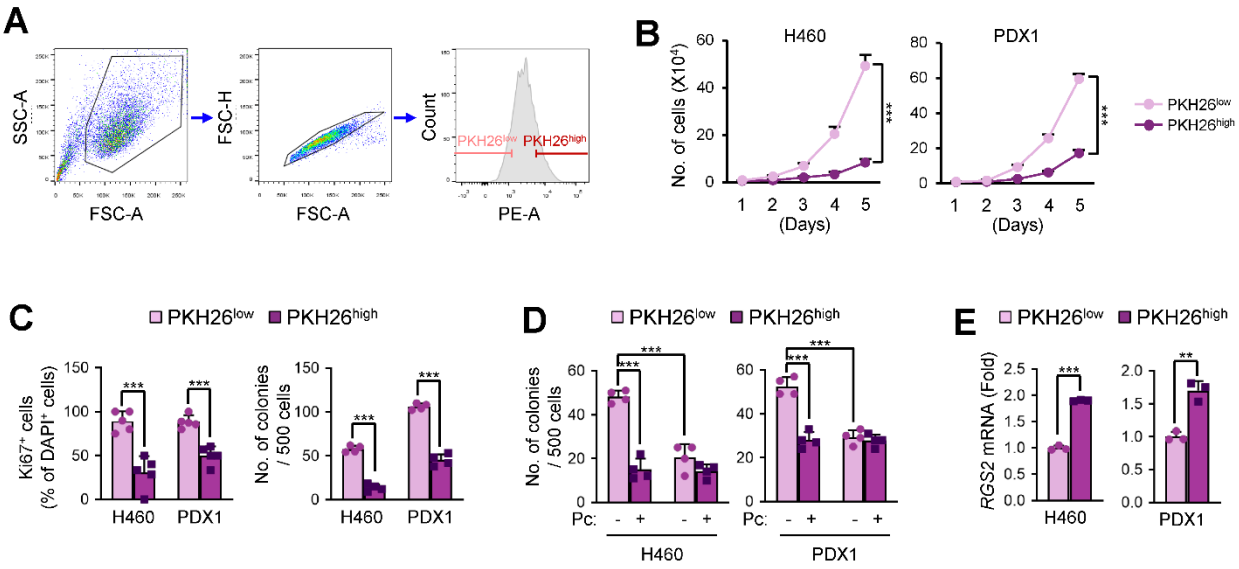

Supplemental Figure 3. Isolation of slow-cycling cell population using PKH26 dye. (**A**) Gating strategy to isolate PKH26^{low} (~10%) and PKH26^{high} (~10%) populations. (**B-D**) Cell proliferation (**B**), basal Ki67 positivity (**C, left**), anchorage-dependent colony formation (**C, right**) and resistance to chemotherapy in the anchorage-independent colony formation assay (**D**) in the PKH26^{low} and PKH26^{high} populations isolated from H460 and PDX1 cells. (**E**) RGS2 mRNA expression level in PKH26^{high} cells compared with PKH26^{low} cells. The data are presented as the means ± SDs. *n* = 3 for **B** and **E**; *n* = 5 for **C left,** *n* = 4 for **C right** and **D**. **P* < 0.05 and ****P* < 0.001, as determined by a two-tailed Student's *t*-test (**B**, **C** and **E**) and one-way ANOVA with Dunnett's post-hoc test (**D**).

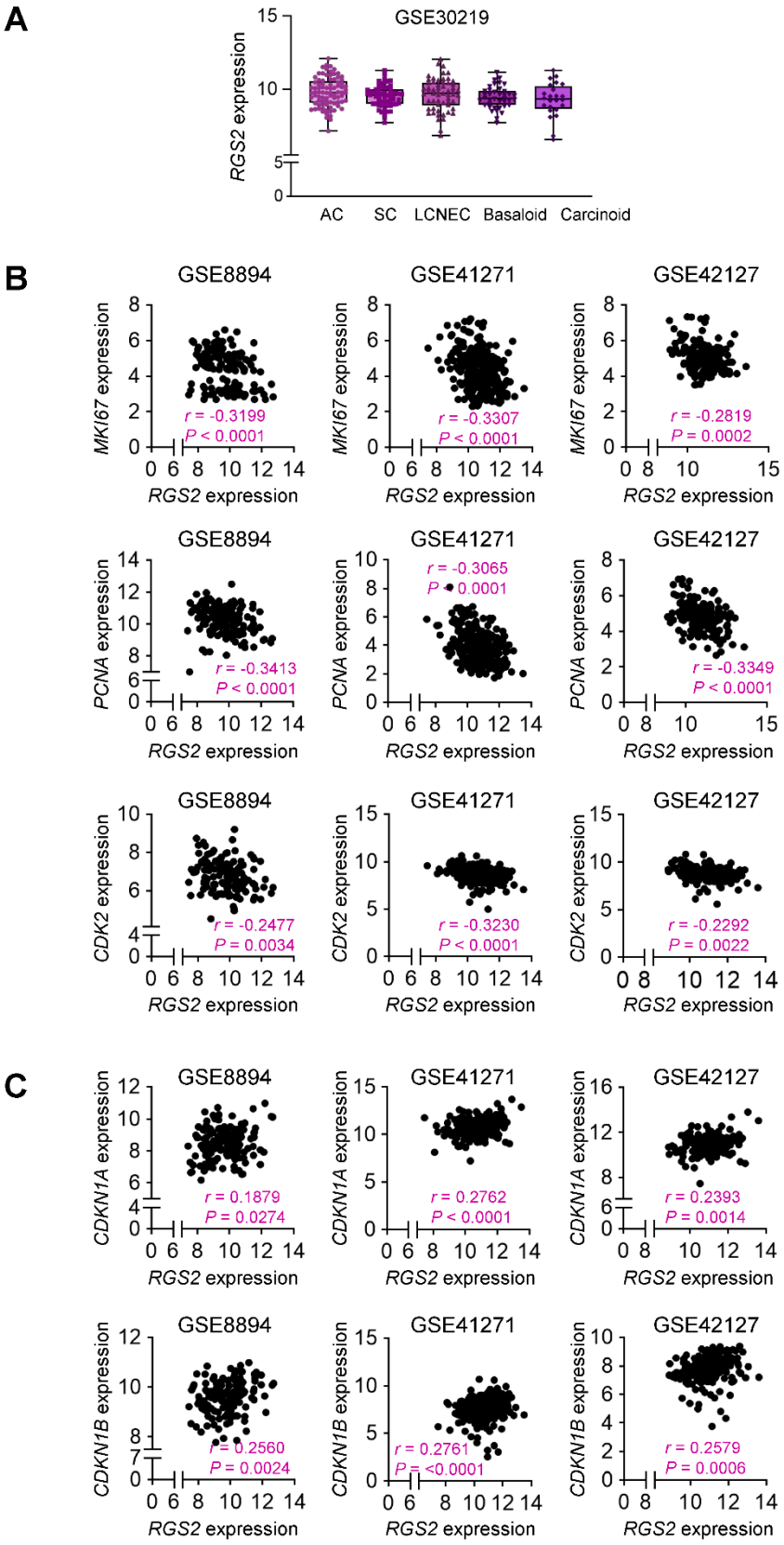

Supplemental Figure 4. Correlations between the expression of RGS2 and cell proliferation-related markers in NSCLC. (**A**) Correlation of *RGS2* expression with NSCLC histology was analyzed by using a publicly available dataset (GSE30219). (**B** and **C**) Pearson and Spearman correlation coefficients were calculated for the correlation analyses between the expression of *RGS2* and that of cellular proliferation markers, such as *MKI67*, *PCNA* and *CDK2* (**B**), and cell cycle regulation markers, such as *CDKN1A* and *CDKN1B* (**C**), in NSCLC using publicly available datasets.

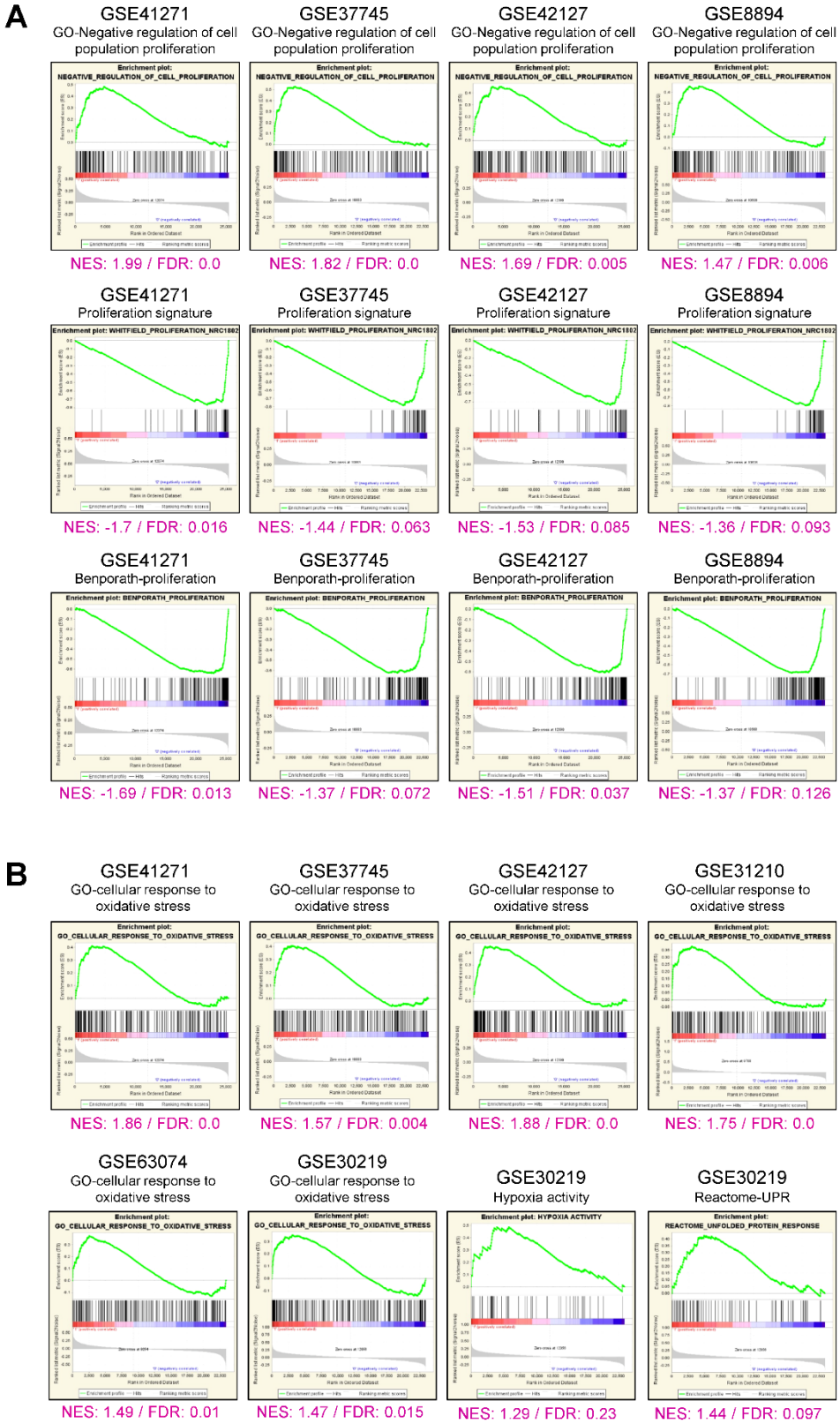

Supplemental Figure 5. Enrichment of cellular proliferation- and stress-associated gene sets in NSCLC tumors with high RGS2 expression. (**A** and **B**) GSEA to determine the enrichment of gene sets related to cell proliferation (**A**) and stress response and UPR (**B**) in RGS2^{high} NSCLC tumors using publicly available datasets. NES: normalized enrichment score. FDR: false discovery rate.

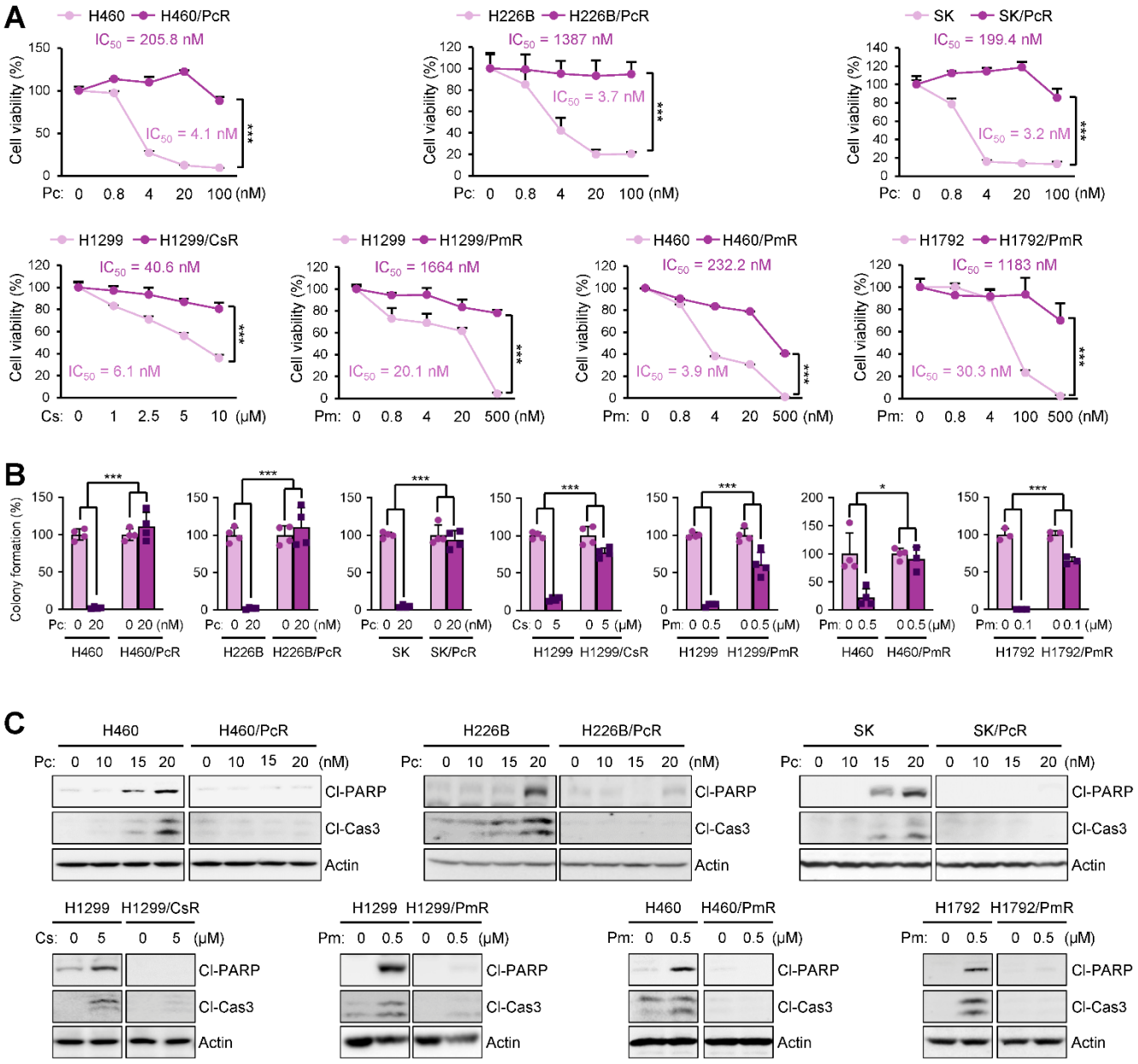

Supplemental Figure 6. Establishment of chemoresistant sublines in NSCLC cell lines. (**A**) The responsiveness of the parental and chemoresistant sublines to chemotherapy was assessed by a cell counting assay (for pemetrexed treatment) or an MTT assay (for paclitaxel or cisplatin treatment). (**B**) Anchorage-dependent colony formation assays were performed to assess the responsiveness of parental and chemoresistant cells to the chemotherapy. (**C**) Immunoblotting showing reduced proapoptotic effects of chemotherapeutic drugs in chemoresistant sublines. Parental [H460, H226B, SK-MES-1 (SK), H1299, and H1792] and chemoresistant (H460/PcR, H226B/PcR, SK/PcR, H1299/CsR, H1299/PmR, H460/PmR, and H1792/PmR) cells were treated with the indicated chemotherapeutic drugs for 2 days. The data are presented as the means ± SDs. n = 3 for **A**; n = 3 or 4 for **B**. *P < 0.05, **P < 0.01, and ***P < 0.001, as determined by a two-tailed Student's t-test Pc: paclitaxel; Cs: cisplatin; Pm: pemetrexed; Cl-Cas-3: cleaved caspase3; Cl-PARP: cleaved poly (ADP-ribose) polymerase.

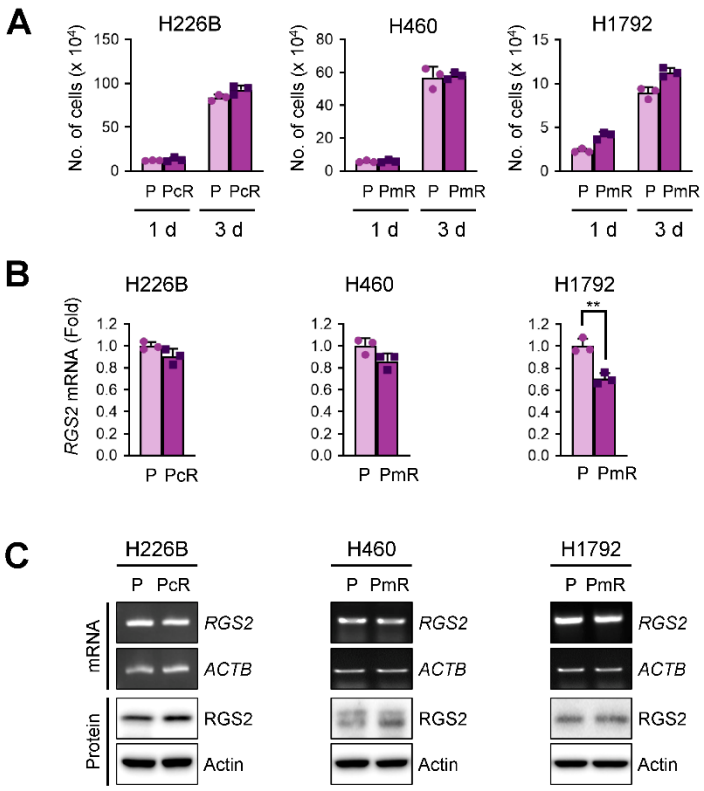

Supplemental Figure 7. Minimal modulation of RGS2 expression in chemoresistant non-SCCs. (**A**) The proliferation of parental ACCs (H226B, H460, and H1792) and non-SCC chemoresistant (H226B/PcR, H460/PmR, and H1792/PmR) cells was assessed by a cell counting assay. (**B** and **C**) The levels of RGS2 mRNA and protein expression in the parental and non-SCC chemoresistant cells were determined by real-time PCR (**B**), RT-PCR and immunoblotting (**C**). The data are presented as the means ± SDs. n = 3 for **A** and **B**. *P < 0.05, **P < 0.01, and ***P < 0.001, as determined by a two-tailed Student's t-test.

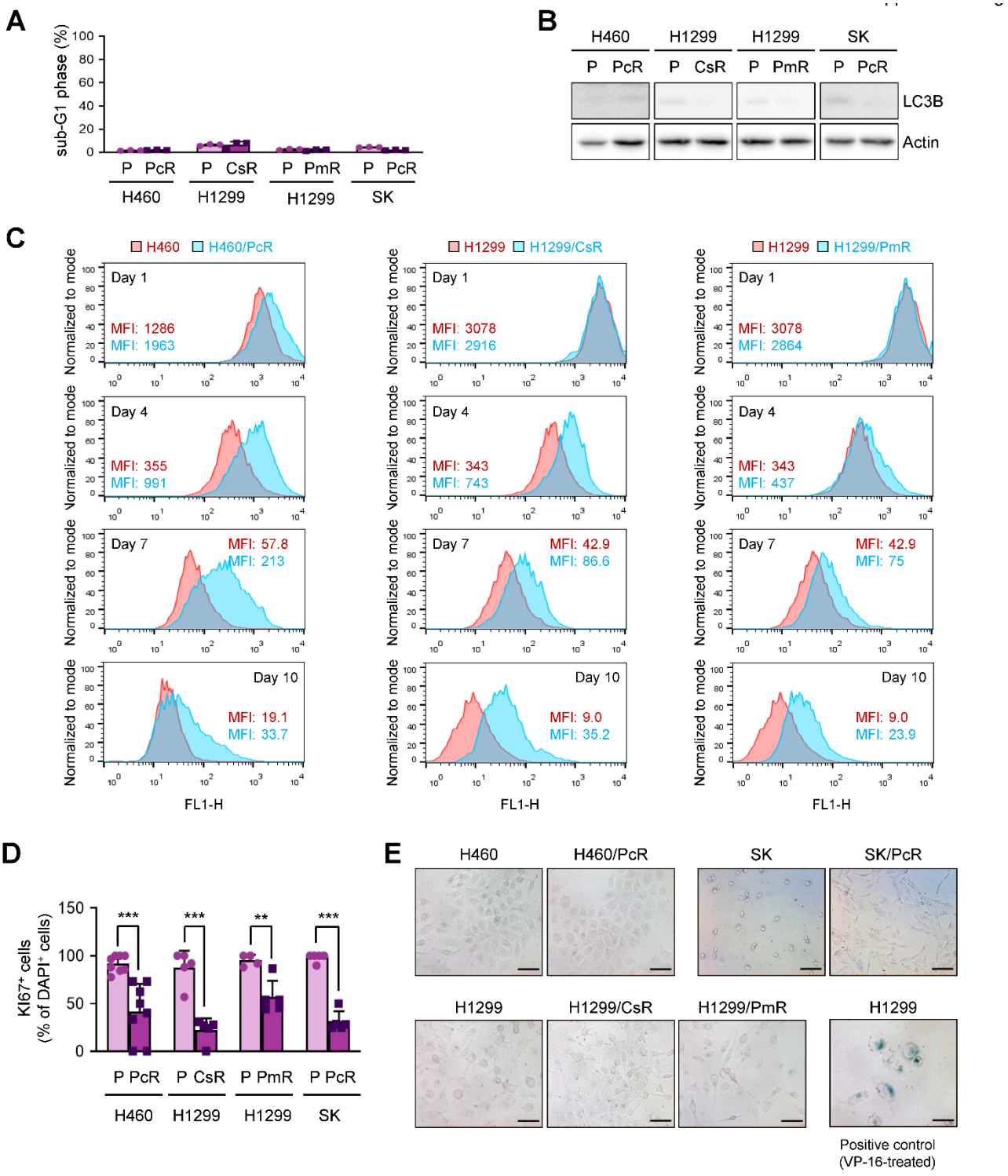
A
sub-G1 phase (%)
P PcR P CsR P PmR P PcR
H460 H1299 H1299 SK
B
H460 H1299 H1299 SK
P PcR P CsR P PmR P PcR
LC3B
Actin
C
H460 H460/PcR
H1299 H1299/CsR
H1299 H1299/PmR
Normalized to mode
Day 1
MFI: 1286
MFI: 1963
MFI: 3078
MFI: 2916
MFI: 3078
MFI: 2864
Day 4
MFI: 355
MFI: 991
MFI: 343
MFI: 743
MFI: 343
MFI: 437
Day 7
MFI: 57.8
MFI: 213
MFI: 42.9
MFI: 86.6
MFI: 42.9
MFI: 75
Day 10
MFI: 19.1
MFI: 33.7
MFI: 9.0
MFI: 35.2
MFI: 9.0
MFI: 23.9
FL1-H
D
KI67+ cells
(% of DAPI+ cells)
P PcR P CsR P PmR P PcR
H460 H1299 H1299 SK
E
H460 H460/PcR SK SK/PcR
H1299 H1299/CsR H1299/PmR H1299
Positive control
(VP-16-treated)
F
Translation+ cells (Fold)
P PcR
H460
P CsR
H1299
P PmR
H1299
P PcR
SK
P PcR
P CsR
P PmR
P PcR

Supplemental Figure 8. Cellular properties of quiescence-like SCCs. (**A**) The basal populations of nonviable ACCs (H460/P, H1299/P, and SK/P) and SCCs (H460/PcR, H1299/CsR, H1299/PmR, and SK/PcR) were determined by flow cytometry. (**B**) Minimal expression of the autophagy marker LC3B in the ACCs and SCCs was determined by immunoblotting. (**C**) Changes in the cellular levels of the CFSE fluorescence in ACCs (H460 and H1299) and SCCs (H460/PcR, H1299/CsR and H1299/PmR) up to 10 days were monitored by flow cytometry at the indicated time point. MFI: mean fluorescence intensity. (**D**) Downregulation of the Ki67-positive cell population in SCCs compared with the corresponding ACCs. (**E**) SA-β-gal activity in parental ACCs (H460, SK, and H1299) and SCCs (H460/PcR, SK/PcR, H1299/CsR, and H1299/PmR) was determined by β-galactosidase staining as described in Supplemental Methods. Scale bars, 100 μm. (**F**) Downregulated nascent protein synthesis in SCCs compared with the corresponding ACCs. Scale bars, 200 μm. The data are presented as the means ± SDs. n = 3 for **A**; n = 4-8 for **D**; n = 3-8 for **F**. *P < 0.05, **P < 0.01, and ***P < 0.001, as determined by a two-tailed Student's t-test.

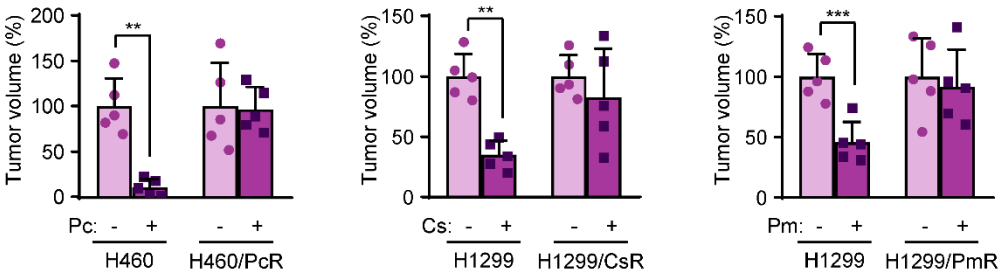

Supplemental Figure 9. Chemoresistant phenotypes of SCCs in vivo. NOD/SCID mice bearing chemoresistant SCCs (H460/PcR, H1299/CsR, and H1299/PmR) or the corresponding parental ACCs (H460 and H1299) were treated with paclitaxel (Pc; 20 mg/kg), cisplatin (Cs; 3 mg/kg) or pemetrexed (Pm; 50 mg/kg) for 2-3 weeks. The tumor volumes in each group at the experimental endpoint are shown. n = 5 per group. The data are presented as the means ± SDs. *P < 0.05, **P < 0.01, and ***P < 0.001, as determined by a two-tailed Student's t-test. Pc: paclitaxel; Cs: cisplatin; Pm: pemetrexed.

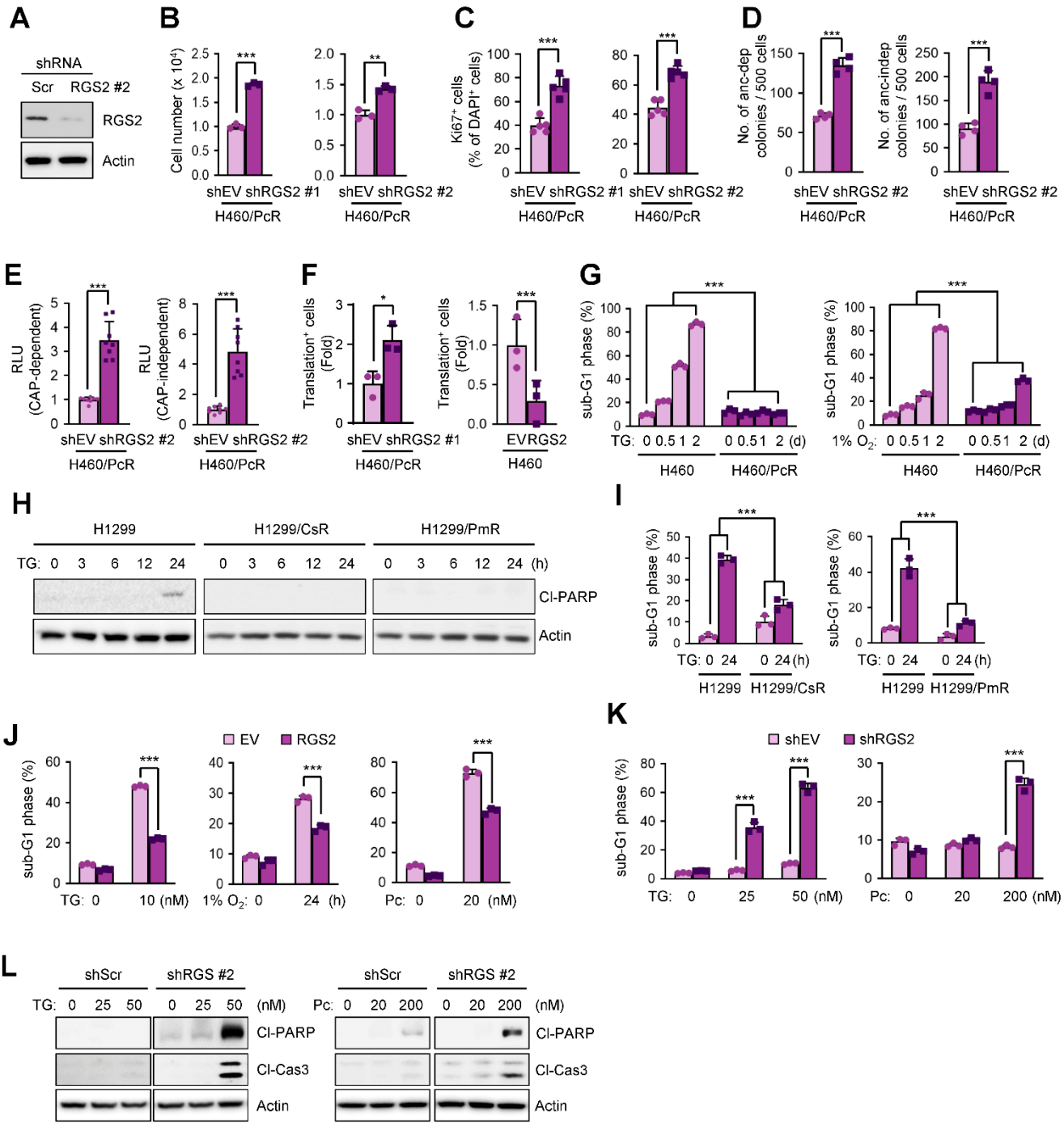

Supplemental Figure 10. Enhancement of cell proliferation, translation, protein synthesis and stress-induced apoptosis by silencing of RGS2 expression and reduction in thapsigargin-mediated apoptosis in SCCs. (**A**) Immunoblotting showing downregulation of RGS2 expression by stable transfection with additional shRGS2 clone (shRGS2 #2) in H460/PcR cells. (**B-E**) Cell proliferation (**B**), basal Ki67 positivity (**C**), anchorage-dependent (**D, left**) and -independent colony formation (**D, right**) and CAP-dependent and -independent translation (**E**) were analyzed in RGS2 knocked down H460/PcR cells (H460/PcR-shRGS2 #1 and #2) compared with scrambled shRNA-transfected H460/PcR cells (H460/PcR-shEV). (**F**) Changes in nascent protein synthesis in H460/PcR-shRGS2 compared with H460/PcR-shEV (**F, left**) or H460 cells stably transfected with RGS2 expression vectors (H460-RGS2) compared with those stably transfected with empty vectors (**F, right**). (**G**) ER stress-induced apoptosis caused by thapsigargin treatment (TG; 25 nM) or hypoxia (1% O_2) in H460 and H460/PcR cells was determined by flow cytometric analysis of the accumulation of sub G1 phase cells. (**H** and **I**) Decreased apoptotic cell death caused by treatment with TG in SCCs (H1299/CsR and H1299/PmR) compared with the corresponding parental ACCs (H1299) was determined by immunoblotting (**H**) and flow cytometric (**I**) analyses. (**J** and **K**) Modulation of UPR-induced apoptosis in H460-RGS2 (**J**) and H460/PcR-shRGS2 cells (**K**) by comparison with H460-EV and H460/PcR-shEV cells, respectively. Apoptosis was determined by flow cytometry analysis. (**L**) Immunoblotting showing enhancement of thapsigargin (TG; 25 nM) or

paclitaxel (Pc; 20 nM)-induced apoptosis in H460/PcR-shRGS2 #2 cells compared with H460/PcR-shScr cells after treatment for 24 h. The data are presented as the means ± SDs. *n* = 3 for **B**, **F**, **G**, **I**-**K**; *n* = 5 for **C**; *n* = 4 for **D**, *n* = 8 for **E**; **P* < 0.05, ***P* < 0.01, and ****P* < 0.001, as determined by a two-tailed Student's *t*-test (**B**-**G, I**-**K**).

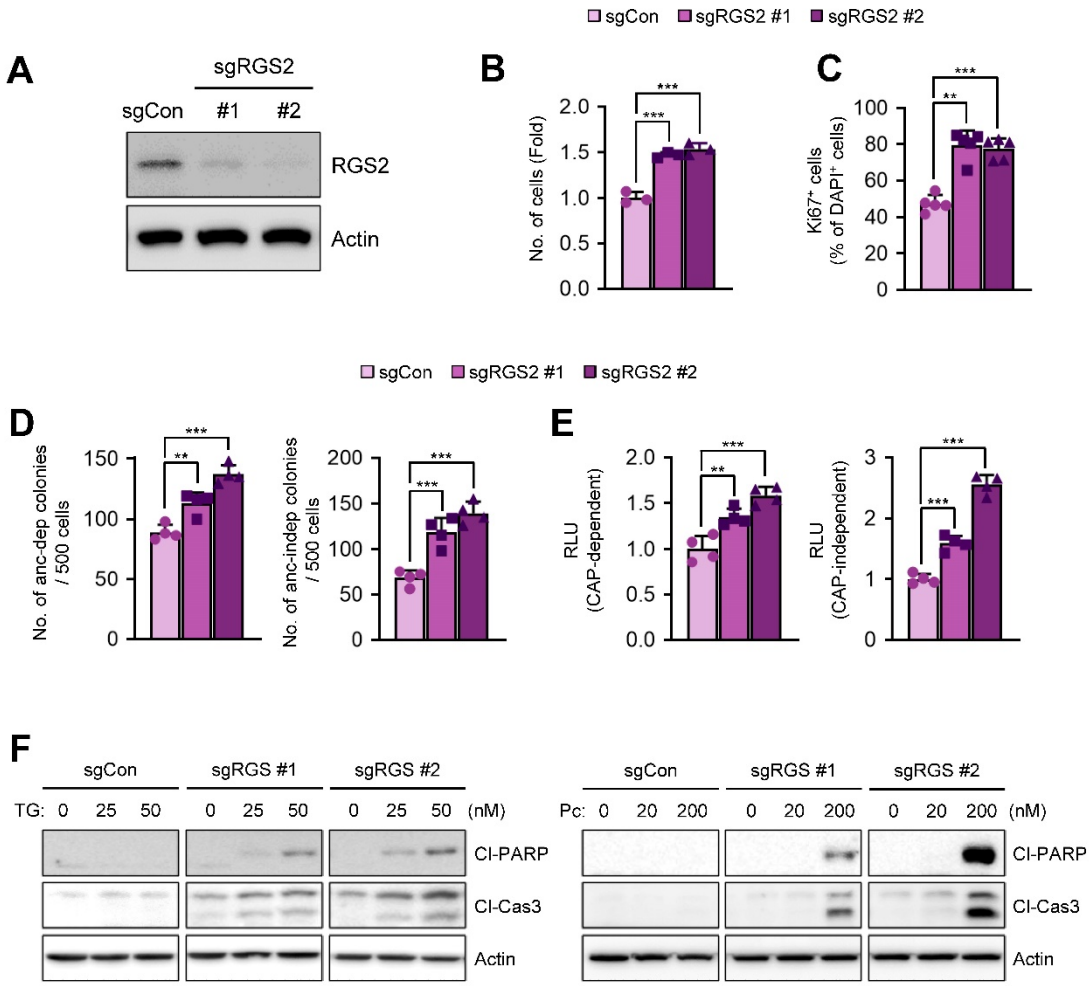

Supplemental Figure 11. CRISPR/Cas9-mediated RGS2 knockout alters slow-cycling and chemoresistant characteristics of SCCs. (**A**) Immunoblotting showing downregulation of RGS2 expression by stable transfection with two different sgRGS2 clones (sgRGS2 #1 and #2). (**B**-**E**) Cell proliferation (**B**), basal Ki67 positivity (**C**), anchorage-dependent (**D, left**) and -independent colony formation (**D, right**), and CAP-dependent and -independent translation (**E**) in two different H460/PcR subclones stably transfected with sgRGS2 #1 and #2 compared with those stably transfected with empty vector (sgCon). (**F**) Immunoblotting showing enhancement of TG or Pc-induced apoptosis in two RGS2 knockout H460/PcR cells treated with indicated concentrations of TG (25 nM) or Pc (20 nM) for 24 h. The data are presented as the means ± SDs. n = 3 for **B**; n = 5 for **C**; n = 4 for **D** and **E**. *P < 0.05, **P < 0.01, and ***P < 0.001, as determined by one-way ANOVA with Dunnett`s post hoc test (**B**-**E**)

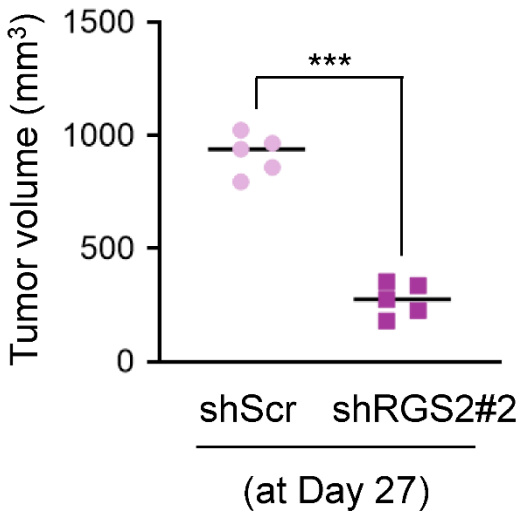

Supplemental Figure 12. Reduced tumor volume in RGS2 knocked down tumors. Reduction of tumor growth in NOD/SCID mice implanted with H460/PcR-shRGS2 #2 cells compared with those implanted with H460/PcR-shScr cells (n = 5 per group). The data are presented as the means ± SDs. *P < 0.05, **P < 0.01, and ***P < 0.001, as determined by a two-tailed Student's t-test.

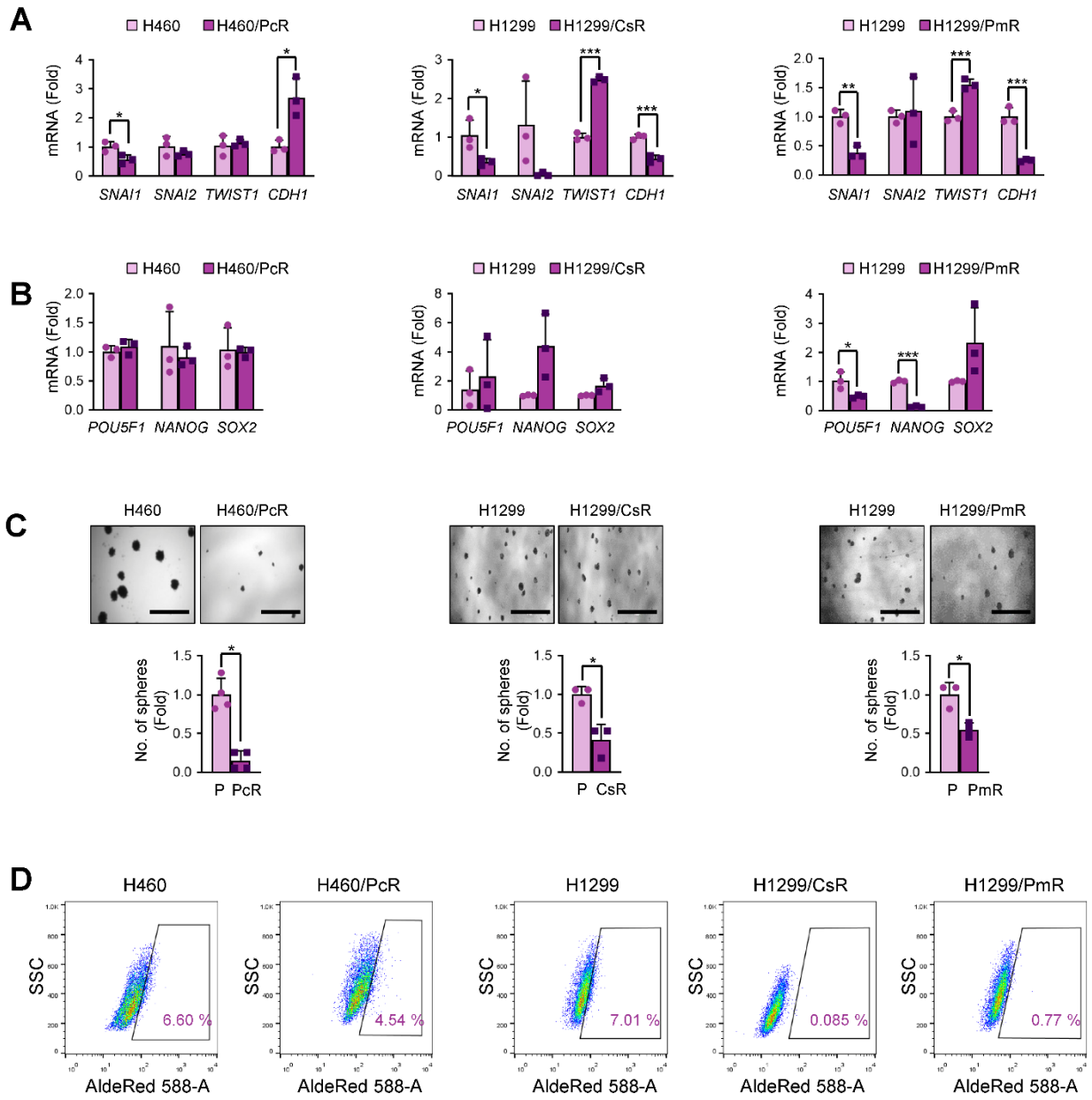

Supplemental Figure 13. Minimally changed EMT and cancer stemness related gene expressions and cancer stem cells phenotypes in SCCs. (**A** and **B**) Changes in the expression of EMT- (**A**) and stemness-related markers (**B**) in SCCs compared with the corresponding ACCs were analyzed by real-time PCR. (**C**) Images showing the sphere-forming ability of ACCs and SCCs under spheroid culture conditions. The number of spheres is shown as a graph. Scale bars, 200 μm. (**D**) ALDH activity-positive ACCs and SCCs were identified by flow cytometric analysis as described in the Supplemental Methods. The data are presented as the means ± SDs. *n* = 3 for **A** and **B**; *n* = 3 or 4 for **C**.**P* < 0.05, ***P* < 0.01, and ****P* < 0.001, as determined by a two-tailed Student's *t*-test (**A-C**).

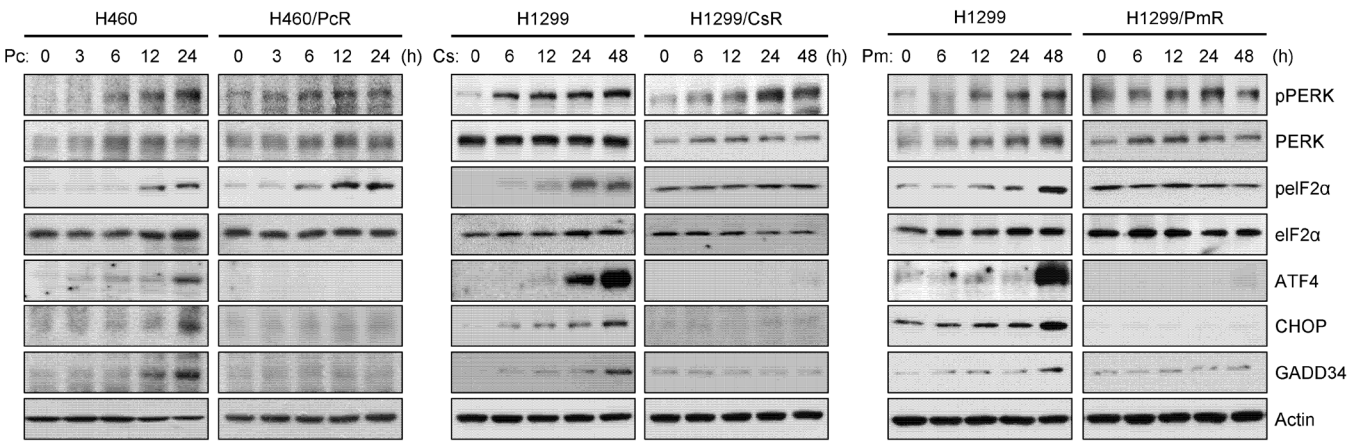

Supplemental Figure 14. Reduction in chemotherapy induced UPR in SCCs. Decreased UPR induction by treatment with chemotherapy [paclitaxel (Pc; 20 nM), up to 24 h ; cisplatin (Cs; 5 μM) and pemetrexed (Pm; 500 nM), up to 48 h] in SCCs (H460/PcR, H1299/CsR and H1299/PmR) compared with the corresponding ACCs (H460 and H1299) was determined by immunoblotting.

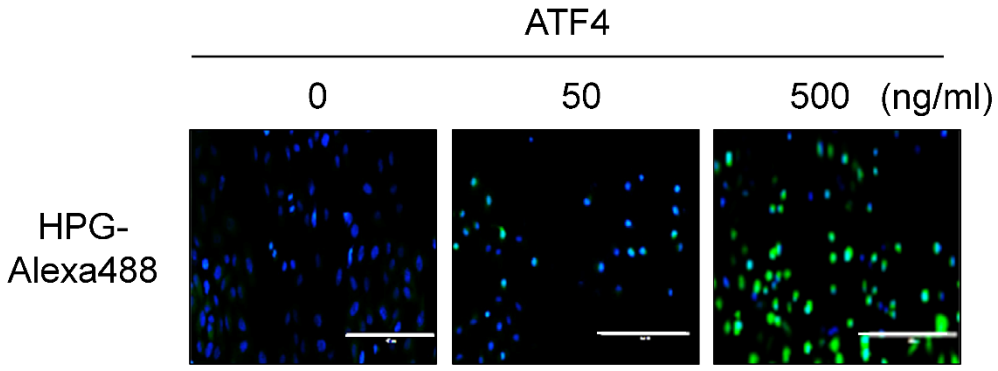

Supplemental Figure 15. ATF4 induces nascent protein synthesis. Nascent protein synthesis in H460/PcR cells transfected with increasing amount of ATF4 was analyzed as described in Methods. Representative immunofluorescence image is shown. Quantification result is shown in **Figure 5F**. Scale bar, 200 μm.

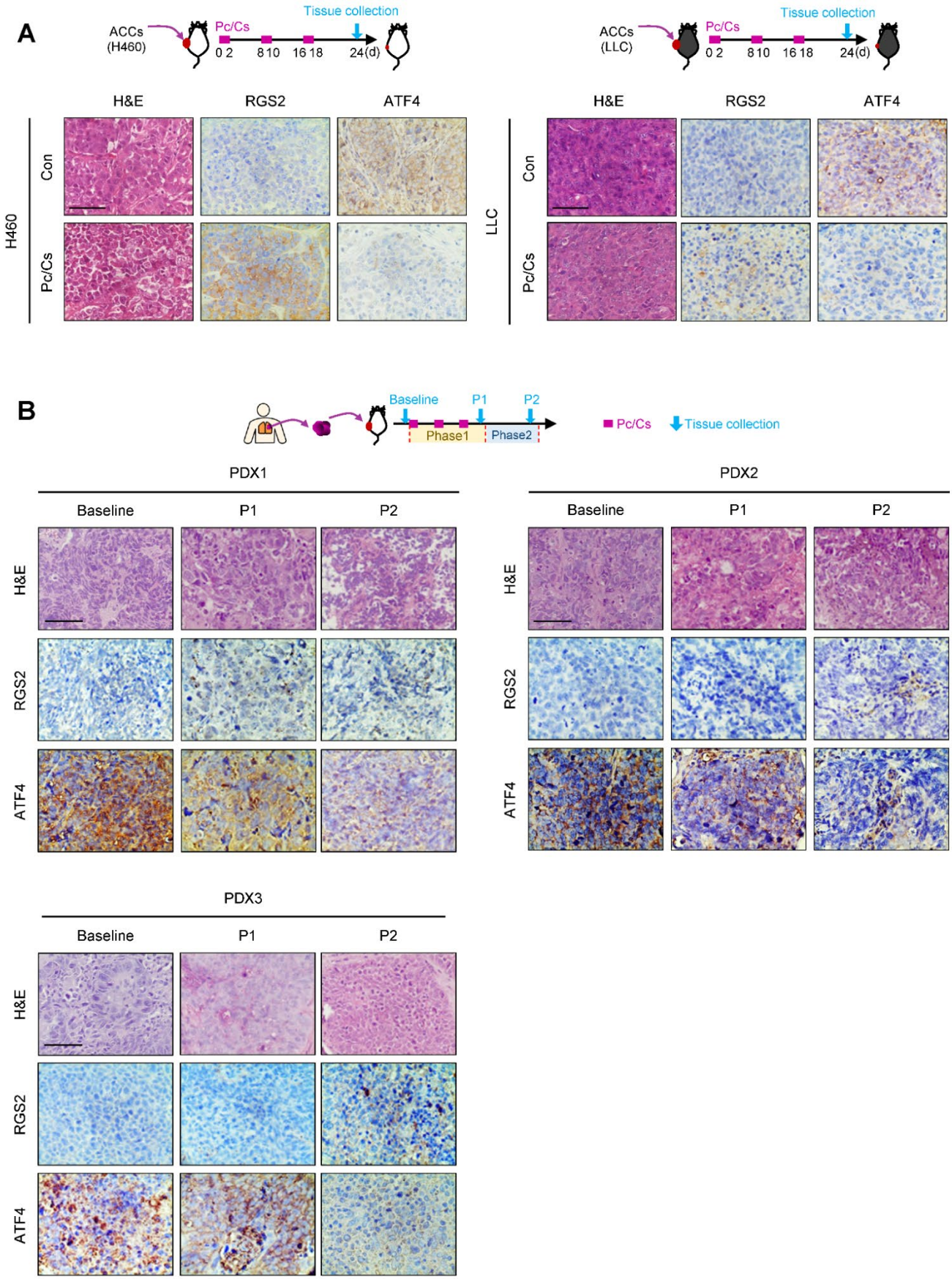

Supplemental Figure 16. Inverse correlation between RGS2 and ATF4 expression in tumors in each phase of chemotherapy treatment. (**A** and **B**) IHC analysis showing upregulation of RGS2 expression and concurrent downregulation of ATF4 expression in tumor tissues from mice treated with chemotherapy. (**A**) Representative H&E and IHC result for RGS2 and ATF4 from H460 and LLC tumors treated with control or Pc/Cs are shown. Quantitative analyses of the IHC images are shown in **Figure 7C and Figure 7G.** Scale bar, 50 μm. (**B**) Representative H&E and IHC result for RGS2 and ATF4 from PDX tumors in each phase of chemotherapy treatment. Quantitative analyses of the IHC images are shown in **Figure 7L**. Scale bars, 50 μm (**A** and **B**).

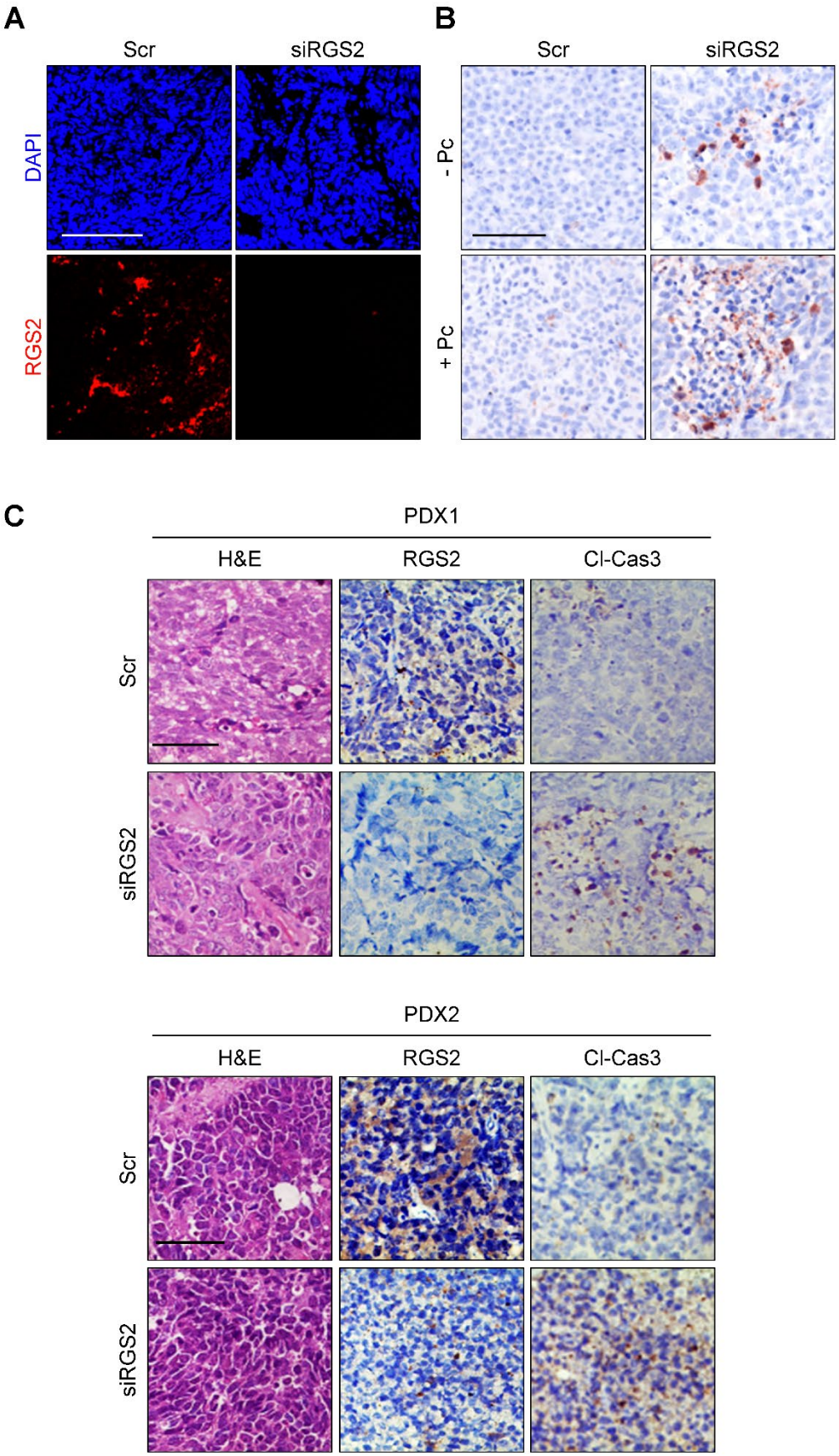

Supplemental Figure 17. RGS2 ablation suppressed tumor relapse by inducing apoptosis. (**A**) Immunofluorescence result showing RGS2 knock down in the tumor treated with RGS2 siRNA compared with tumors treated with scrambled siRNA. Scale bar, 20 μm. (**B**) H460/PcR xenograft tumors were harvested after intratumoral RGS2 siRNA injection in combination with paclitaxel treatment. Representative IHC results for Cl-Cas3 were shown. Quantification result is present in **Figure 8E**. Scale bar, 100 μm. (**C**) Representative IHC results for Cl-Cas3 in relapsed tumors treated with intratumoral scrambled or RGS2 siRNA. Quantification results are shown in **Figure 8G**. Scale bar, 50 μm.

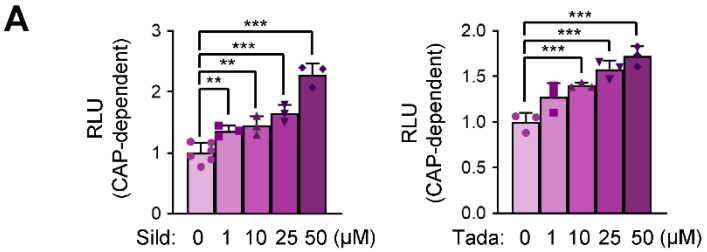
A
RLU (CAP-dependent)
Sild: 0 1 10 25 50 (μM)
Tada: 0 1 10 25 50 (μM)

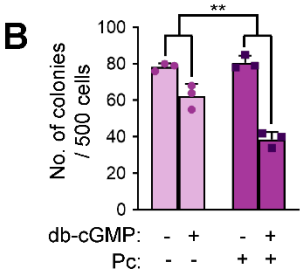
B
No. of colonies / 500 cells
db-cGMP:
Pc:

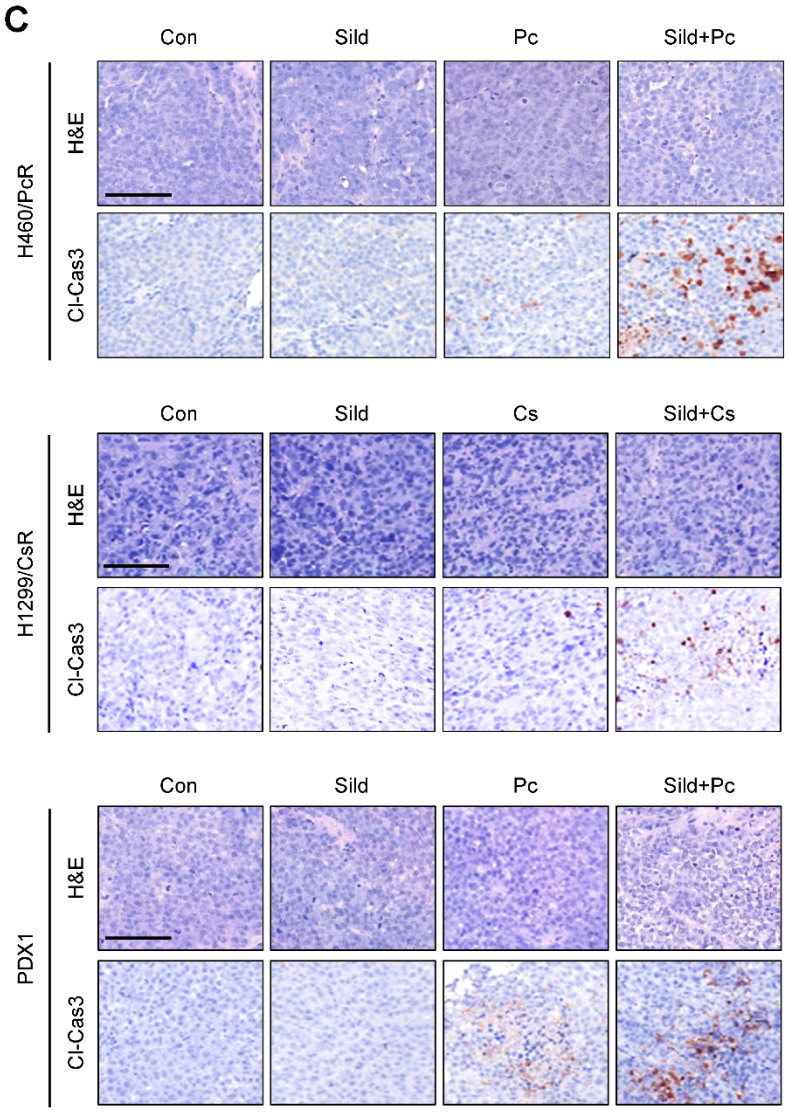
C
Con
Sild
Pc
Sild+Pc
H460/PcR
H&E
Cl-Cas3
Cs
Sild+Cs
H1299/CsR
PDX1

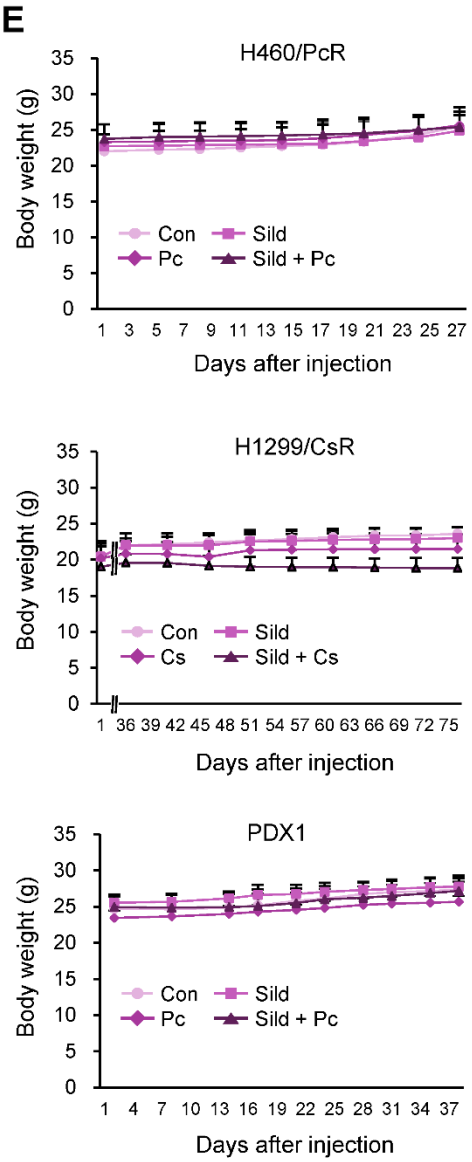
E
H460/PcR
H1299/CsR
PDX1
Body weight (g)
Con
Sild
Pc
Cs
Sild + Pc
Sild + Cs
Days after injection

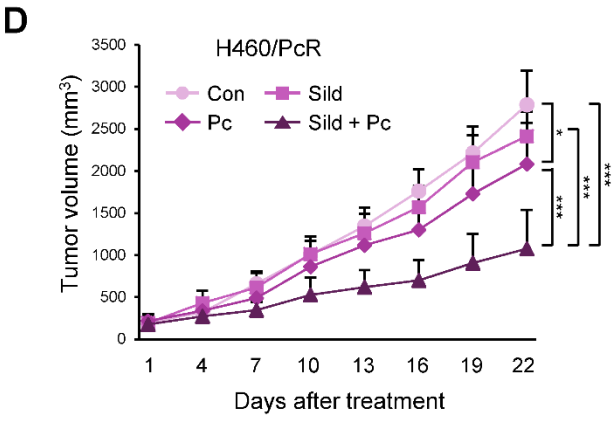
D
H460/PcR
Con
Sild
Pc
Sild + Pc
Tumor volume (mm3)
Days after treatment

Supplemental Figure 18. Upregulation of protein translation by elevation of cGMP levels and enhanced apoptosis by combinatorial treatment with chemotherapy and sildenafil with no overt toxicity. (**A**) Upregulation of protein translation in H460/PcR cells by treatment with the PDE5 inhibitors, sildenafil (Sild) or tadalafil (Tada). (**B**) Anchorage dependent colony formation of H460/PcR cells treated with either db-cGMP alone or in combination with paclitaxel (Pc; 20 nM). (**C**) IHC staining for cleaved-caspase3 (Cl-Cas3) in tumors treated with a combination of chemotherapy and sildenafil. Scale bars, 100 μm. (**D**) Enhancement of tumor growth inhibition by combined treatment with sildenafil (10 mg/kg) and paclitaxel (20 mg/kg) in NOD/SCID mice bearing established H460/PcR xenograft tumors (~200 mm^3). (*n* = 7 per group). (**E**) Mice were treated with vehicle or chemotherapeutic drugs [paclitaxel (Pc; 20 mg/kg) or cisplatin (Cs; 3 mg/kg)] in the presence or absence of sildenafil (Sild; 10 mg/kg) for 4-19 weeks. The body weight changes in mice in each treatment group are shown as a graph. The data are presented as the means ± SDs. *n* = 3-6 for **A**; *n* = 3 for **B**.*$P < 0.05$, **$P < 0.01$, and ***$P < 0.001$, as determined by one-way ANOVA with Dunnett's post-hoc test (**A**, **B** and, **D**).

Figure 3D

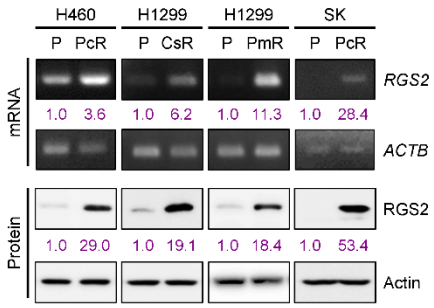

Figure 3E

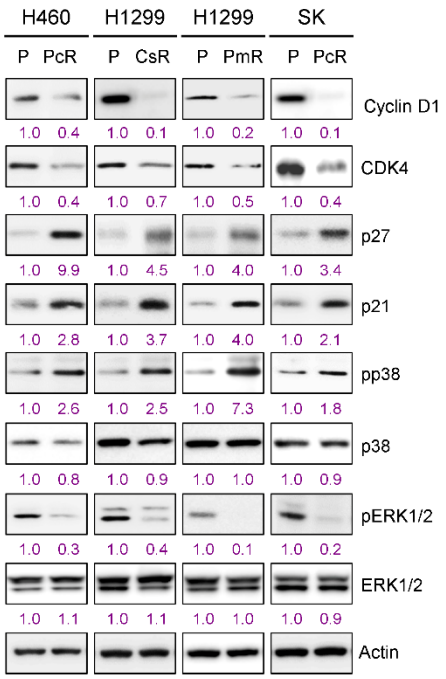

Figure 4B

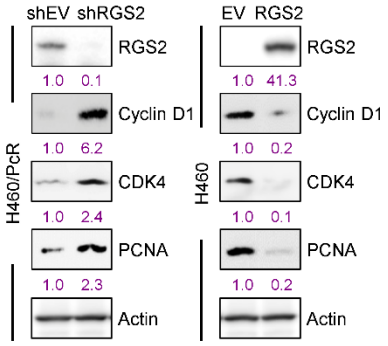

Figure 4E

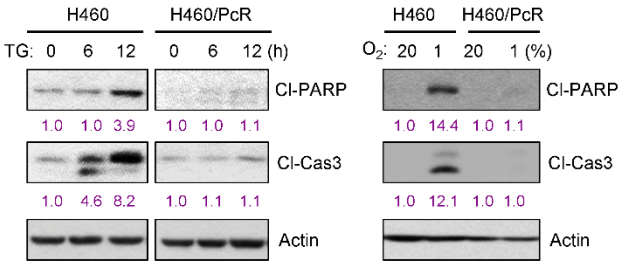

Figure 4F

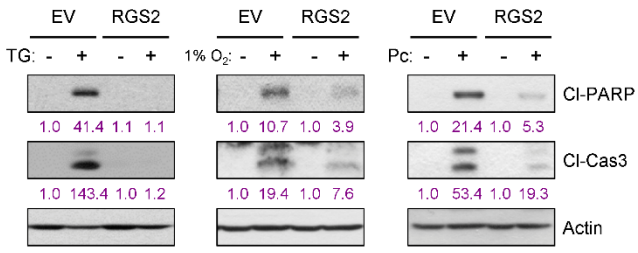

Figure 4G

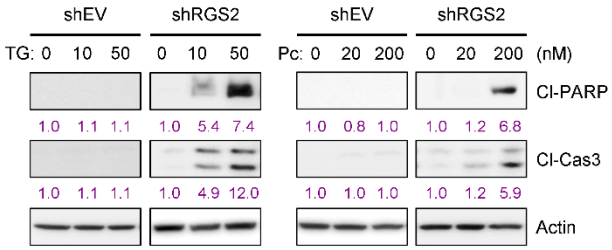

Supplemental Figure 19. Immunoblot images with the band intensities

Figure 5B

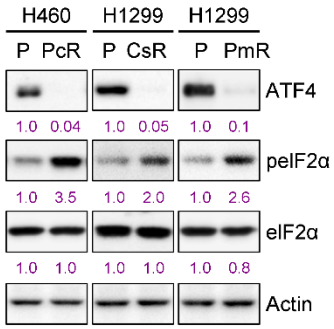

Figure 5C

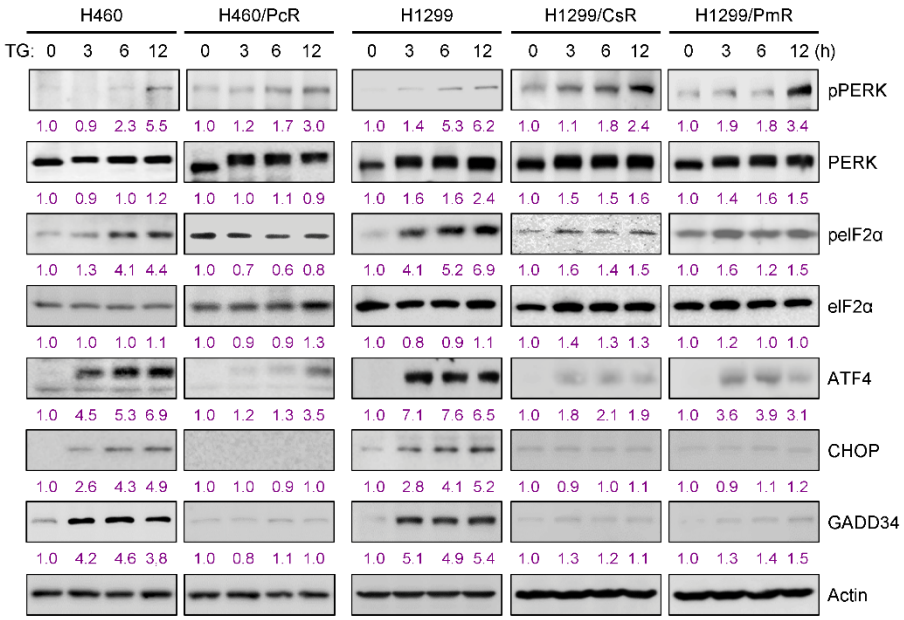

Figure 5H

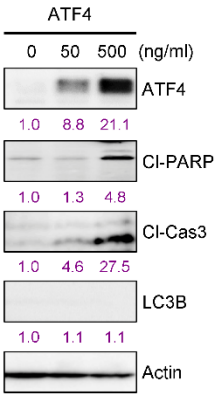

Figure 5I

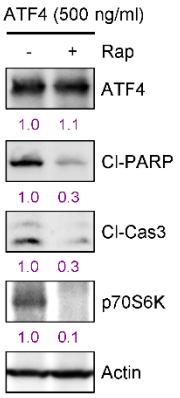

Figure 5J

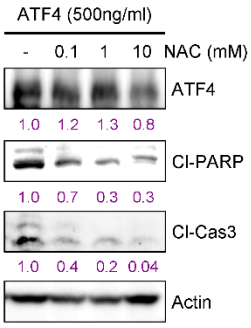

Figure 6A

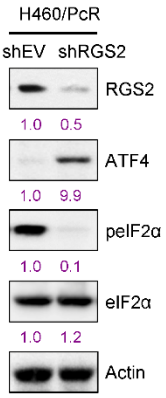

Figure 6B

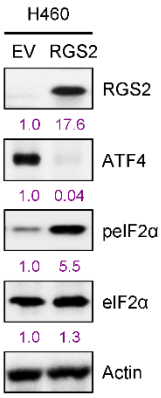

Supplemental Figure 19. (Continued)

Figure 9A

Figure 9D

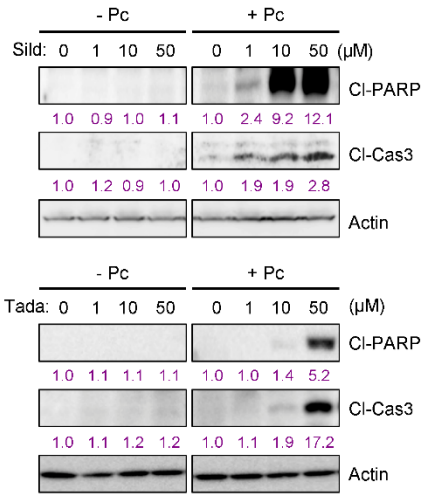

Figure 9E

Figure 9F

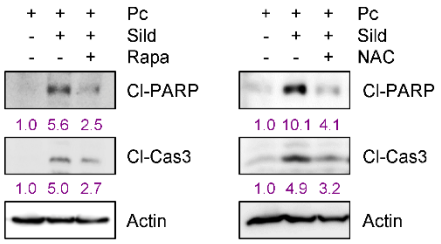

Supplemental Figure 19. (Continued)

Supplemental Figure 6C

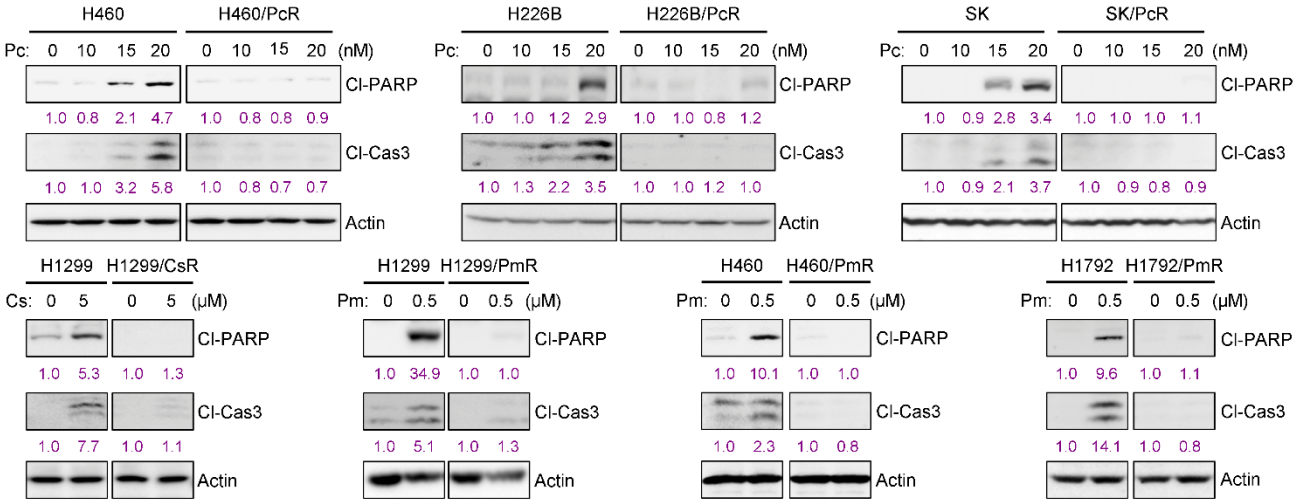

Supplemental Figure 7C

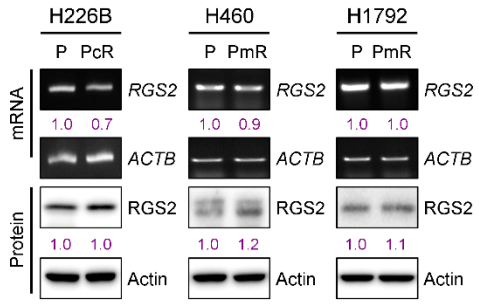

Supplemental Figure 8B

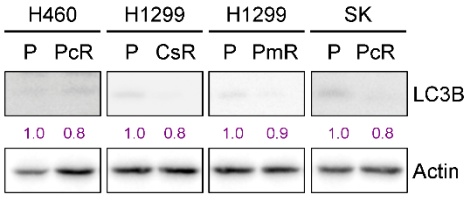

Supplemental Figure 10A

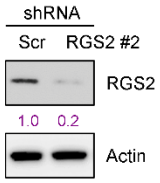

Supplemental Figure 10H

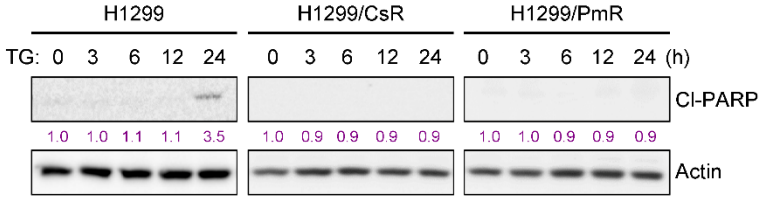

Supplemental Figure 10L

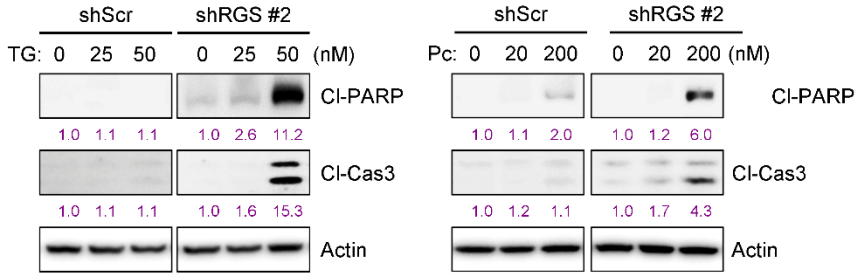

Supplemental Figure 11A

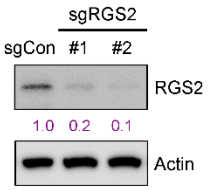

Supplemental Figure 11F

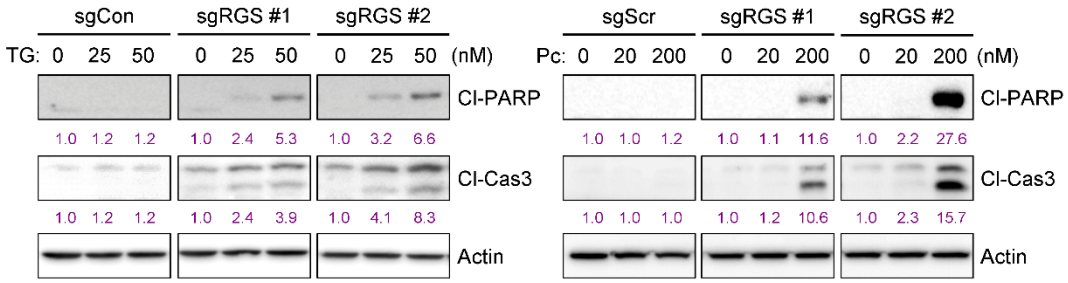

Supplemental Figure 19. (Continued)

Supplemental Figure 14

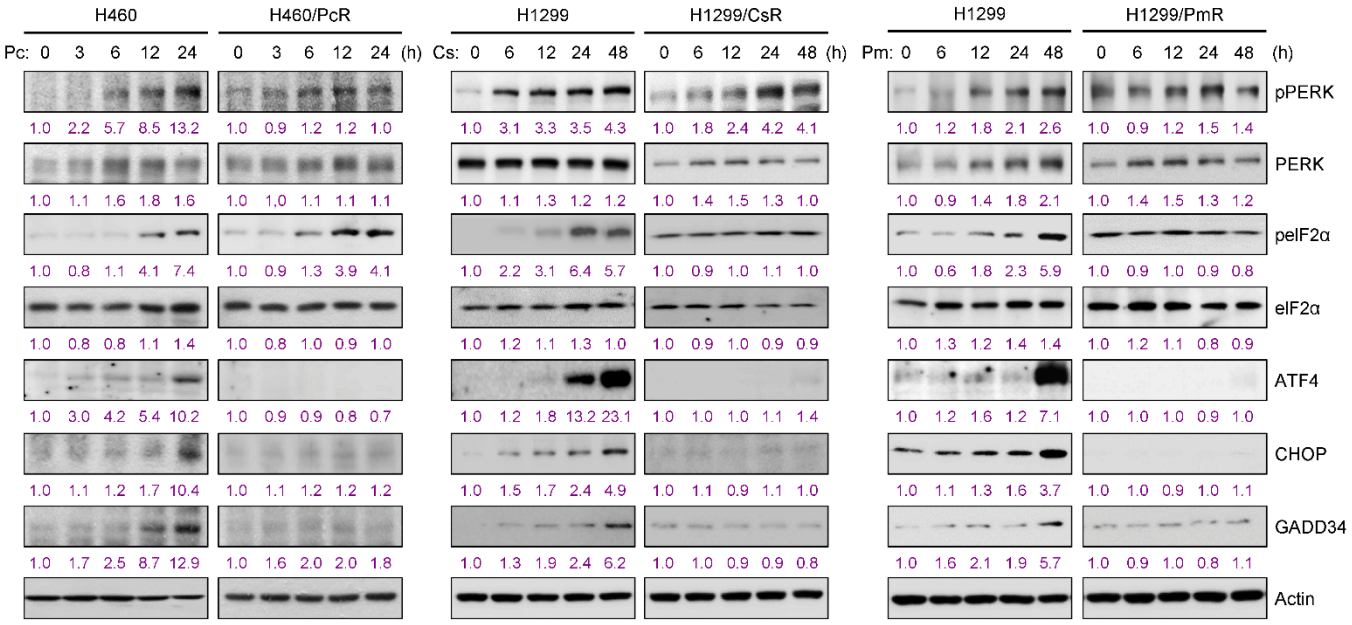

Supplemental Figure 19. (Continued)